SEASONAL & INTER-ANNUAL VARIABILITY OF OBSERVED MESOSCALE EDDIES IN THE CARIBBEAN SEA

MARGARITA EUGENIA LÓPEZ ALZATE

ESCUELA NAVAL DE CADETES ALMIRANTE PADILLA

FACULTAD DE OCEANOGRAFÍA FÍSICA

PROGRAMA DE MAESTRÍA EN OCEANOGRAFÍA

CARTAGENA DE INDIAS, D. T. Y C.

2020

SEASONAL & INTER-ANNUAL VARIABILITY OF OBSERVED MESOSCALE EDDIES IN THE CARIBBEAN SEA

MARGARITA EUGENIA LÓPEZ ALZATE

DEGREE PROJECT AS A PARTIAL REQUIREMENT TO QUALIFY FOR

MASTER IN OCEANOGRAPHY

SUPERVISORS:
PHD JUAN MANUEL SAYOL

PHD ALEJANDRO ORFILA

ESCUELA NAVAL DE CADETES ALMIRANTE PADILLA

FACULTAD DE OCEANOGRAFÍA FÍSICA

PROGRAMA DE MAESTRÍA EN OCEANOGRAFÍA

CARTAGENA DE INDIAS, D. T. Y C.

2020

NOTA DE ACEPTACIÓN

FIRMA DEL DIRECTOR

FIRMA DEL CODIRECTOR

FIRMA DEL EVALUADOR

FIRMA DEL EVALUADOR

To our passion: the Ocean

"... How are we fal'n, fal'n by mistaken rules?
And Education's, more than Nature's fools,
Debarr'd from all improve–ments of the mind,
And to be dull, expected and designed;
And if some one would Soar above the rest,
With warmer fancy, and ambition press't,
So strong th' opposing faction still appears,
The hopes to thrive can ne'er outweigh the fears ..."

Countess of Winchilsea Anne Finch, *"The Introduction"*

Acknowledgments

Henceforth I will remember this Thesis as “The opportunity”. Opportunity to understand, accept and trust in Academy, System and Society. To me, they were necessary actions to take the next step: learning, understanding and researching the Ocean. Life is about processes... and this has been my own.

“Happy are those who dream dreams and are ready to pay the price to make them come true.”
–Leon Joseph Suenens

Let’s talk about the price: I opened my eyes and my mind to a correct understanding. There were no possibility to pay this fair price by myself, and, this the reason why I want this thesis to be reminded as the opportunity to start to appreciate the world from another perspective. With “the world” I mean, again, Academy, System and Society. This other perspective I am talking about is Professor Alejandro Orfila’s view and his way to do Science and to nurture student’s confidence; this perspective is what makes me conclude that research should be an honest team, the system must be transparent and society have to be empathetic.

Life is about processes where, beside opening and closing doors, we must make the decision to cross them. In the middle of my process, Prof. Orfila introduced myself to PhD Juan Manuel Sayol who, without knowing me, not only opened one door for me but pushed me to come in, to trust and to fall in love again with science.

For both of you: *“... más que admiraciones, en vez de gracias, diciendo que no soy capaz de agradeceros la más mínima parte de lo que os debo. (...) Especial favor de que conozco ser su deudora, como de otros infinitos de su inmensa bondad; (...) Y así, cuando esto considero acá a mis solas, suelo decir: Bendito seáis vos, Señor, que no sólo no quisisteis en manos de otra criatura el juzgarme, y que ni aun en la mía lo pusisteis, sino que lo reservasteis a la vuestra, y me librasteis a mí de mí y de la sentencia que yo misma me daría –que, forzada de mi propio conocimiento, no pudiera ser menos que de condenación–, y vos la reservasteis a vuestra misericordia ...”* (Sor Juana Inés de la Cruz, 1691)

A mis padres Consuelo y Jorge Iván, otra vez: ha sido una fortuna en mi vida tenerlos como padres. Gracias por su amor, su apoyo, tolerancia y comprensión, pero sobretodo gracias por transmitirme sus principios y la convicción de que con amor y perseverancia se puede alcanzar lo que te propongas, incluso sueños.

When dreams begin to come true...

¡ G R A C I A S !

Abstract

Mesoscale eddies are ubiquitous features in the ocean that typically exhibit different properties respect to their surroundings transporting passive tracers such as heat, salt and carbon, and being relevant structures for the redistribution of energy and mass around all the oceans. Eddies also play an important role in supplying nutrients to the shelf-slope and to the upper layers where phytoplankton blooms may result. More than one half of the kinetic energy of the ocean dynamics is contained in the mesoscale, in which eddies are the major player. In this Thesis the main statistical characteristics of mesoscale eddies in the Caribbean Sea as well as the seasonal and inter-annual variability in the number of eddy observations are studied. Since the Caribbean Sea is a semi enclosed basin, a large part of the transport of nutrients and heat both in the vertical and in the horizontal are to a large extent the result of these structures. Key descriptors of mesoscale eddies from satellite-based sea level anomalies (SLA) such as their lifetime, size and amplitude are assessed for the period between 1993 and 2016. Moreover, the spatio-temporal variability in the number of eddy observations is evaluated against the Sea Surface Temperature (SST), the surface wind curl and the main climatic index of variability in the area, El Niño Southern Oscillation (ENSO). The ENSO appears to have certain influence at the inter-annual scale in the number of eddy observations. The above analysis is performed by combining a suite of statistical techniques such as the power spectral density, the coupled Singular Value Decomposition, Self-Organizing Maps and the wavelet transform. The more accurate knowledge of the main eddy properties, and the spatio-temporal variability of the number of eddy observations provided in this thesis, contributes to understand better their formation and dissipation mechanisms and their preferred trajectories, who have crucial implications on the biogeochemical cycles as well as on some air-sea exchange processes in the Caribbean Sea.

Keywords: mesoscale eddies, Caribbean Sea, ENSO, seasonal, inter-annual, connectivity

Research line: Mesoscale dynamics at seasonal and inter-annual time scales
Secondary research line: ENSO variability

x

Contents

List of Figures

List of Tables

Chapter 1

Introduction

1.1 Background

Ocean coherent mesoscale eddies are features that can be interpreted as analogous to the high and low pressure systems that we see daily on the weather channel (Chelton et al., 2007). These structures have a size of around 10 to 200 km and a lifetime from weeks to several months which indeed define their "mesoscalar" nature. Strictly speaking, the definition of an eddy includes all coherent vortexes as well as a rich cascade of other objects such as filaments, squirts and spirals. These objects are characterized by density, temperature and/or salinity fronts with associated flow anomalies that are nearly in geostrophic balance (Gaube et al., 2015). Mesoscale eddies are ubiquitous in all world oceans, allowing the transport of heat, salt, nutrients and carbon around the ocean (Morrow and Traon, 2012). A significant part of the kinetic energy of the ocean circulation is contained in the mesoscale coherent eddies, while the remainder is largely distributed into other structures with smaller live-times (filaments, fronts, small eddies) and in the large-scale circulation. Eddies can also feed energy and momentum back into the mean flow enhancing the deep ocean circulation.

The largest eddies emerge from instabilities of strongly horizontally sheared motions, particularly in boundary currents. These eddies often take the form of well defined rings that extend to great depths. Depending on which side they form, eddies contain either relatively warm or cold water compared to their surroundings and they rotate anticyclonically or cyclonically respectively (in the Northern Hemisphere, the opposite in the Southern Hemisphere). Anticyclonic eddies display a central sea surface height (SSH) higher (by few to tens of centimeters) than outer waters while cyclonic eddies present a SSH lower than in the surroundings. The cyclonic (anticyclonic) eddy is characterized by a cold (warm)-core eddy or ring. Warm-core eddies can actually trap and transport a wide variety of aquatic life within them but the cold-core eddies tend to have a greater amount of biological activity. Winds from the overlying atmospheric circulation can produce surface currents that sometimes cause convergence or divergence patterns of upper ocean

waters of several kilometers in scale. Under the right divergent conditions, cool, nutrient-rich waters can upwell from deeper layers to act as a seed for the formation of a cold-core eddy, and warmer, nutrient-poor waters may converge and be downwelled to forming a warm-core eddy. Moreover, in the last decades many studies have demonstrated that eddies affect the atmospheric boundary layer by increasing convection (warm eddies) or stabilizing the atmosphere (cold eddies), specially at those regions with very strong sea surface temperature (SST) fronts, which at the same time can alter the cloudiness and the rain rate (e.g. Liu et al., 2017).

Eddies can extend downwards into the ocean for hundreds (even thousands) of meters lasting from weeks to months or even more than a year. Under favorable background conditions they can travel hundreds or thousands of kilometers albeit at a slow forward speed, acting as key mechanisms for mass, momentum and energy redistribution across the oceans. In addition to their role in moving heat horizontally, mesoscale eddies also transfer heat vertically in the ocean, specially during their formation from baroclinic instabilities where they tilt isopycnals, largely moving heat upwards to partially compensate the downward heat transport by time mean fields.

Early oceanographic observations of mesoscalar eddies were made in the 1930's by Columbus Iselin and colleagues during quarterly Montauk-to-Bermuda cruises (Cullen, 2005). The first intentional measurements of an eddy were made during the 10-day occupation of a cold-core, cyclonic Gulf Stream ring in the 1940's (Iselin and Fuglister, 1948). It was not until the mid-1960ś that the first study dedicated solely to the dynamics of these eddies was completed marking the beginning of the scientific investigation of mesoscale meanders and eddies.

Today, eddies of few tens of km and larger can be observed from satellites, providing a global coverage at near weekly intervals. SSH signatures of eddies are measured by satellite altimeters merging observations from simultaneously operating altimeters (Chelton et al., 2007, 2011a). The impact of eddies on marine phytoplankton became apparent in 1978 with the launch of the Coastal Zone Color Scanner, one of eight instruments flown aboard the Nimbus-7 satellite. This early proof-of-concept mission operated intermittently for 91 months and led the way for follow-on missions, resulting in the rich archive of bio-optical observations from the visible portion of the electromagnetic spectrum available today.

The Caribbean Sea is not exempt from the apparition of eddies and is known to have a large temporal and spatial variability (Carton and Chao, 1999). The main circulation in the Caribbean Sea is characterized by the throughflow of the wind-driven subtropical North-Atlantic gyre known as the Caribbean Current (Johns et al., 2002). The origin of the Caribbean Current waters is diverse: from the North Atlantic, the South Atlantic

and nearby Amazon and Orinoco Rivers (Jury, 2011). The main flow is affected at seasonal and inter-annual time scales by regional differences in wind stress (Andrade, 2000; Oey and Lee, 2003), resonating Rossby waves (Hughes et al., 2016) and by large scale climatic variability such as El Niño Southern Oscillation (ENSO) or the Pacific Decadal Oscillation (Alvera-Azcarate and Barth, 2009; Beier et al., 2017).

Several studies have been carried out to describe how mesoscale eddies form, propagate and dissipate in the Caribbean region using ship-drift, buoys, drifters, satellite-based observations and numerical models. Caribbean Sea eddies may potentially be playing an important role in the North Atlantic circulation by exchanging mass and momentum with the surrounding waters (Carton and Chao, 1999). Many authors have shown that the mesoscale variability in this region is dominated by anticyclonic eddies (Molinari et al., 1981; Centurioni and Niiler, 2003; Richardson, 2005; van der Boog et al., 2019). Most of them form in the eastern side of the Caribbean Sea, transporting salinity anomalies as a result of the Amazon and Orinoco river plumes westward (van der Boog et al., 2019). On the other hand, other authors have related the development of eddies with the flow-topography interaction (Molinari et al., 1981), the meandering current (Andrade and Barton, 2000), instabilities due to the presence of river plumes (Chérubin and Richardson, 2007) and perturbations caused by the interaction of boundary currents with topography (Goni and Johns, 2003; Jochumsen et al., 2010). Some of these works concluded that the flow in the Caribbean Sea is intrinsically unstable, which means that any perturbation could trigger the formation of eddies (Jouanno et al., 2008).

After their formation, eddies are advected westward in the Caribbean by the mean flow (Andrade and Barton, 2000) affecting completely the ecosystem as they transport larvae and nutrients offshore (Andrade and Barton, 2005; Baums et al., 2006). The advection of these eddies mainly formed by cold filaments also leads to a cooling of the Caribbean Sea interior (Jouanno and Sheinbaum, 2012). During their propagation, eddies become more energetic (Carton and Chao, 1999; Andrade and Barton, 2000; Richardson, 2005; van der Boog et al., 2019). Although this intensification is evident in observations (Carton and Chao, 1999; Pauluhn and Chao, 1999; Andrade and Barton, 2000; Richardson, 2005), only few studies have elaborated (although shortly) the dynamics of this intensification (van der Boog et al., 2019). Based on surface drifter data, Richardson (2005) suggested that the anticyclonic shear of the Caribbean Current could amplify the anticyclones. In contrast, Andrade and Barton (2000) found, based on satellite altimetry data, a direct relationship between the maximum curl of the wind stress and the westward intensification of anticyclones. This relationship highlights that wind stress alters the life cycle of the anticyclones. Jouanno et al. (2009) used a regional model to study the life cycle of Caribbean anticyclones and computed the mechanical energy balance of the flow in this region. Although this balance shows that baroclinic instabilities provide the necessary energy for the westward growth of anticyclones, it does not explain what drives the

westward intensification of anticyclones. More recently, van der Boog et al. (2019) have attributed the westward intensification of anticyclonic eddies to mainly the salinity gradients generated by upwelling events and river outflow combined with the westward rise of the background velocity shear. Altogether strengthens the thermal wind balance within the vortex.

Despite the importance of these structures, to date there has not been done a systematic census of eddies in the Caribbean Sea, nor evaluating their seasonal and inter-annual variability, spatial distribution, size, etc.

1.2 Caribbean Sea

1.2.1 Dynamics of the Caribbean Sea

The Caribbean is a semi-enclosed sea of the western Atlantic Ocean, extending between 8°N – 25°N and 85°W – 55°W (Fig. 1.1, left panel). It is confined on the south and west by South and Central America, on the east and north by the chain of Antilles Islands Arc, with many passages and divided into Greater and Lesser Antilles (Fig. 1.1, right panel), and the Atlantic Ocean (Andrade, 2000; Johns et al., 2002; Richardson, 2005; Jury, 2011). Regarding the bottom topography, the Caribbean Sea can be divided into five basins (See Fig. 1.1, left panel): between the Lesser Antilles Arc and Las Aves Ridge lies the Granada Basin, the Venezuelan Basin in the east and the Colombian Basin in the west which are separated by The Beata Ridge which crosses the central Caribbean, The Central American Rise separates the Cayman and Colombian Basins, and the Cayman Ridge divides the Cayman and Yucatan Basins. The Caribbean Sea ends at the north in the Yucatan Strait (Andrade, 2000).

The most important sources of water inflow in the Caribbean Sea are provided by the returning deep southwestwards waters from the Gulf Stream, which have three different contributions: the North Equatorial Current passing through the Leeward Islands of the Lesser Antilles (∼8 Sv), the flows in the Windward Passage between Cuba and Hispaniola (∼7 Sv) and the current through the Mona Passage between Hispaniola and Puerto Rico (∼ 3 Sv). On the southeastern edge, the North Brazil Current (NBC) bears fresh water from the Orinoco River, flowing northwestward into the Caribbean basin through the "Windward Island" -in the passages of Grenada (∼6 Sv) and St. Vincent and St. Lucia (∼4 Sv) - forming a coastal current known as the Caribbean Current (Carton and Chao, 1999; Andrade and Barton, 2000; Johns et al., 2002; Richardson, 2005; Jury, 2011).

As mentioned above, south of 15°N the Caribbean inflow is primarily of tropical and south Atlantic origin. South Atlantic waters integrated in the NBC flow northwestward along the continental margin of South America in the form of a coastal current (Richardson, 2005). The NBC curls to the east and south near 6° N from about June through

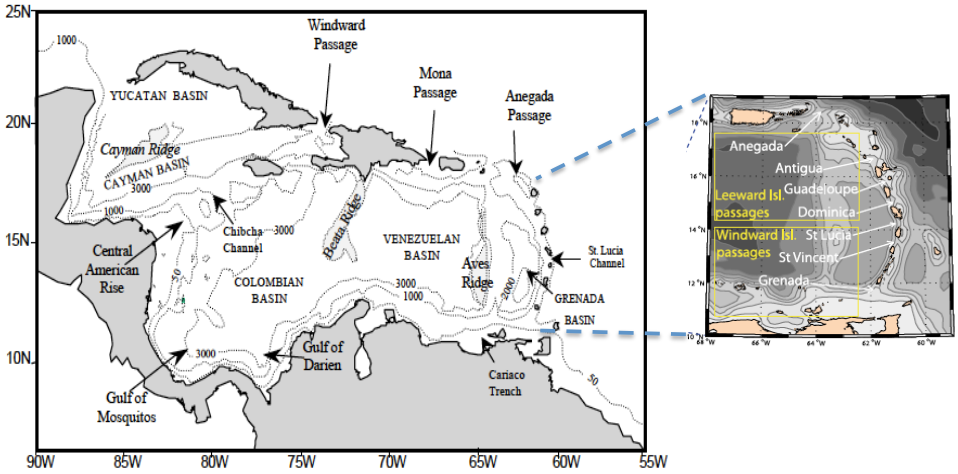

Figure 1.1: Geographic location of the Caribbean Sea with the different basins and bathymetric contours (left panel). The “Antillas” arc closing the basin at the eastern side (right panel). Figures adapted from Rousset and Beal (2011) and Andrade (2000).

March feeding the North Equatorial Countercurrent (NECC) (Hellweger and Gordon, 2002). Periodically, roughly 8–9 times per year, large (400-km diameter) NBC rings pinch off from the retroflection and translate northwestward toward the Caribbean at a speed around 15 cm/s (Richardson, 2005). Most rings travel northward just East of the Antilles to around 14–18°N where the rings stall and decay. During the rest of the year, the NBC continues along the coast to feed the Guyana Current. Both, the Guyana Current and NBC retroflection eddies represent a significant source of water for the Caribbean Sea (Hellweger and Gordon, 2002; Johns et al., 2002).

The bathymetry has a crucial role in the mean circulation of the Caribbean Sea (Alvera-Azcarate and Barth, 2009). The Caribbean Current flows westward at a mean velocity of 0.5 m/s starting where the Guyana Current flows into the Lesser Antilles, and continues forward the northern coast of Venezuela and Colombia (Molinari et al., 1981; Johns et al., 2002; Richardson, 2005). It moves northwest between Nicaragua and Jamaica, with a branch forming the Panama–Colombia cyclonic gyre which is a permanent feature of the Panama–Colombia Basin (Richardson, 2005; Alvera-Azcarate and Barth, 2009). From here, the steering caused by the Nicaraguan Rise obligates the Caribbean Current to first turn sharply north before returning west to form a western boundary current along the eastern coast of Mexico (Alvera-Azcarate and Barth, 2009). Westward currents exit via the Yucatan Channel (in the form of the Yucatan Current) and when they reach the Gulf of Mexico become the Loop Current which receives contributions from the Antilles Current (the westward flow north of the Antilles Islands) and from other Atlantic sources (Andrade, 2000; Johns et al., 2002; Richardson, 2005; Jury, 2011; Alvera-Azcarate and Barth, 2009). The Caribbean Current is the major route by which South Atlantic water flows into the Florida Current and Gulf Stream and is therefore an impor-

tant conduit of the upper part of the northward-flowing meridional overturning circulation (MOC) (Andrade and Barton, 2000; Richardson, 2005).

1.2.2 Climate in the Caribbean Sea

The Caribbean Sea is located in the inter-tropical zone receiving a large amount of solar radiation. The climate in the region is characterized by its thermal homogeneity with a surface air temperature that ranges annually between 21 and 29 °C, which remains constant within a range of 2 to 5°C. Throughout the day, temperature can oscillate within a range of 10 to 15°C between the coolest during the night and the hottest during the day.

The most relevant climatic features in the Caribbean are the Trade Winds from the northeast and the southeast which are developed near surface in the tropical zone as a consequence of the Earth's rotation. The convergence of these winds near the Equator forces the warm equatorial air to rise causing a cooling of the air by thermal expansion, a condition that favors the condensation and the development of clouds forming a zonal band of vigorous convection known as Intertropical Convergence Zone (ITCZ) (Fig. 1.2). The ITCZ is characterized by very unstable atmospheric conditions with a location that varies latitudinally across the Equator with the seasons following the apparent displacement of The Sun with respect to The Earth. The ITCZ moves towards the north of the Equator during the boreal summer and then, it moves to the south, crosses the Equator and moves towards the southern hemisphere.

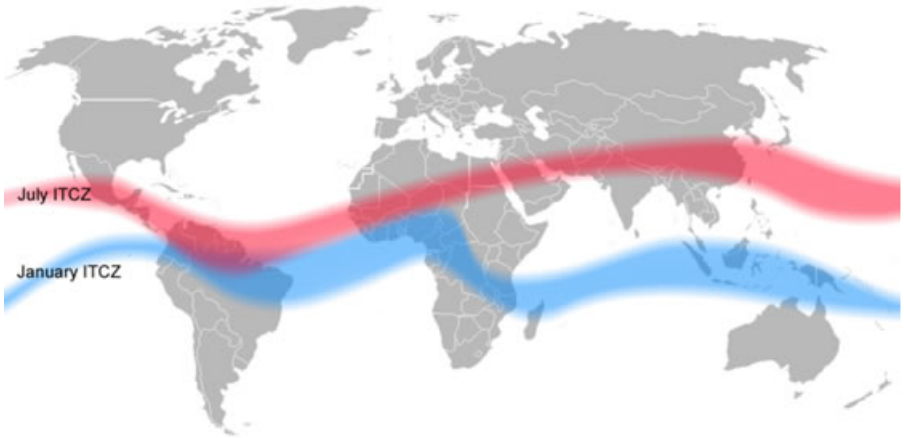

Figure 1.2: Location of the ITCZ in January (blue) and in July (red). (https://www.cioh.org.co/meteorologia/Climatologia

According to the local hydrology two well-marked periods can be defined in the Caribbean region: the rainy and the wet seasons. However, if the wind, temperature and rain are assessed together, a better classification can be made in terms of seasonal coherence;

the both above mentioned (the dry and wet), from December to March and from September to November respectively, a transitional Season, from April to May and the so-called Veranillo de San Juan, from June to August. This seasons are mainly driven by the location of the ITCZ and by the cycle of the American Monsoon System –the meridional movement of the rainy season year round- in the tropics (Andrade and Barton, 2000).

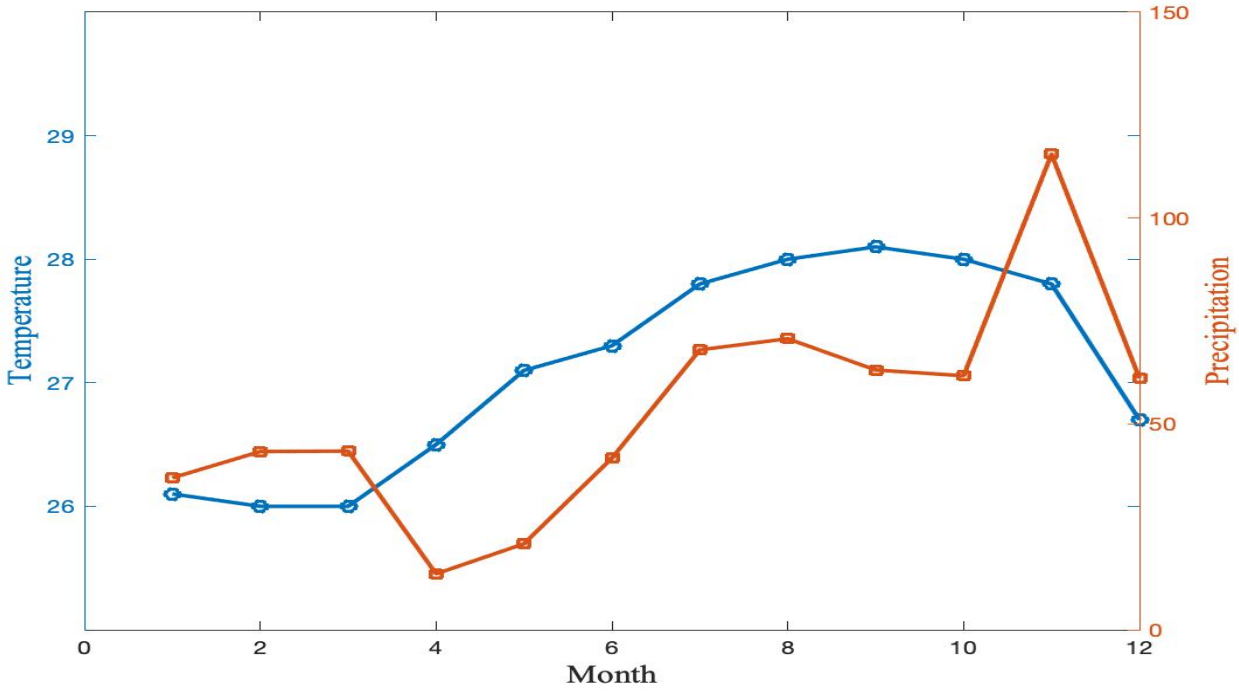

Figure 1.3: Monthly mean temperature blue) and monthly mean precipitation (red line). Data correspond to the period 1950-2000 at $25.75°$ N ,$76°$ W (data downloaded from www.climate.geog.udel.edu)

Monthly temperature and precipitation data in a location off the northern coast of Colombia ($25.72°$ N, $76°$ W) for the period 1950-2000 (Fig. 1.3), show that the minimum temperature occurs during the dry season, to later increase during the following 2 months coinciding with the minimum of precipitation (the transitional season). The following months, from June to August, the temperature and precipitation start to increase defining the Veranillo season (Veranillo de San Juan, because San Juan/Saint John takes place on 24^{th} of June, coinciding with the NH summer solstice) and finally, temperature drops while precipitation increases defining the wet season from September to November. Thus, in this thesis, we will define the year through these four seasons that are characterized as follows:

- *Dry season*: The dry season extends from the month of December to March of the following year. The dry season is the coolest one of the year in the Caribbean Sea, when mean temperatures range between $16°$ and $22°$. In general, the average

number of days with rain is not more than 10 days with light, sporadic and short rains, in which the average rainfall is 71.1 mm (2.8 inches).

In the dry season the ITCZ resides at its southernmost position around 0-5°S. At that time the Northern Hemisphere Trade winds, sometimes called “Easterlies", dominate the area with daily average speeds of about 8 m/s that rise up to 15 m/s during the diurnal maximum (Andrade, 1993). The Trade winds have a southward component in the Colombian Basin during this season. Little or no precipitation occurs during this period.

- *Transitional season*: From April to May; it is common for the Northern Trades to increase temporarily, inhibiting the increasing precipitation rate of the region.
- *Veranillo de San Juan Season*: June to August; the Easterlies weaken and some precipitation occurs with gradual increase in temperature.
- *Wet season*: During the rainy season, from September to November, the ITCZ moves to 10-12°N allowing the Southern Trade winds, sometimes called 'Southerlies', to cross the Central American Isthmus and to reach the Caribbean Basin. The associated winds are weak in the south western Caribbean Sea promoting one of the highest rates of precipitation anywhere around the globe.

1.3 Objectives

The general objective of this Thesis is to characterize statistically mesoscale eddies in the Caribbean Sea and unravel their seasonal and inter-annual variability.

This broad objective will be achieved through 3 specific objectives:

1. Eddy characterization. Development of an Atlas of daily mesoscalar eddy observations in the Caribbean Sea classified by size, polarity, amplitude, rotational and translational speed and by their preferred pathways.
2. Seasonal variability. Analyze the decrease/increase in the number of eddy observations in response to local winds and/or SST.
3. Inter-annual variability. Evaluating the role of the El Niño-Southern Oscillation (ENSO) in the variability of the number of mesoscale eddy observations in the Caribbean Sea.

Chapter 2

Data & Methods

This chapter introduces data and methods used in this Thesis. First, it is described the global mesoscale eddy trajectory atlas derived from sea surface height (SSH), which is a product created after a generic two-step process that includes eddy identification and eddy tracking. Second, satellite-based Sea Surface Temperature (SST) and surface horizontal wind fields are presented. These secondary data will be used to characterize the seasonal and inter-annual variability of eddies in Chapter 4. Moreover, some widely used methods to analyze the spatio-temporal variability of geophysical variables employed in Chapters 3 and 4 to analyze eddy-properties are introduced in this chapter.

2.1 A brief introduction to satellite altimetry

Satellite altimetry is a technique that enables us to map the Earth's topography and, for our interest, the sea surface patterns by measuring the SSH. SSH accounts for the effects of the sea surface height that would exist without any disturbances and dynamic topography (AVISO, 2017), and is computed as the range at a given instant from the sea surface to an ellipsoid that is an approximation to the shape of the Earth. Thus, satellite altimetry measures the altitude of the satellite above the sea surface by radar altimeters at vertical incidence. This radar permanently transmit signals at high frequency (over 1700 pulses per second) toward the sea surface and then reflect them back. Although the objective is to determine the distance from the satellite to a place on the sea surface by measuring the round-trip time of a radar pulse, the magnitude and shape of the waveforms also contain information about the characteristics of the surface which caused the reflection (AVISO, 2017). As a result, this technique allows to monitor mesoscale features by measuring the sea surface anomaly around which currents swirl by the geostrophic balance between pressure gradient and Coriolis force, which has enormous implication for to estimate, among others, heat, salt or chlorophyll storage and transport (Cipollini and Snaith, 2013).

2.2 Eddy Trajectory Atlas

We employ the AVISO Mesoscale Eddy Trajectory Atlas Product (AVISO, 2017) to perform eddy statistics in the Caribbean Sea. This product provides information on mesoscale eddies derived from altimetry-based sea level anomalies (SLA). It has been produced by SSALTO/DUACS and distributed by AVISO+ with support from CNES, in collaboration with Oregon State University with support from NASA. To create this eddy tracking product, the processing uses DUACS "two satellite" daily Delayed Time Gridded Sea Level Anomalies product, originally distributed by AVISO + (the product is available after registration at: website AVISO +). The bone of the algorithms used were largely based on the original codes implemented at Oregon State University.

Due to current wavelength limitations of altimetric sensors, mesoscale eddies are identified as features with diameters of 100-300 km. The larger scale variability has been removed using a low pass filter (a second order Lanczos filter). The result was subtracted from the original SLA data to produce a grid that only contains mesoscale variability (AVISO, 2017). The period covered by this product extends from January 1993 to December 2016, and provides some information on each detected eddy such as radius, amplitude, rotational speed, polarity (cyclonic/anticyclonic) as well as the time when it was observed, the coordinates of the estimated center, the track identification or the observation number.

2.2.1 Eddy identification

Many methods have been proposed to identify eddies: either based on the analysis of SSH fields (e.g. Chelton et al., 2011b; Mason et al., 2014; Faghmous et al., 2015), the winding angle (e.g. Chaigneau et al., 2008), on the estimation of parameters related with relative vorticity (e.g. Henson and Thomas, 2008), the instantaneous Lagrangian flow (e.g. Beron-Vera et al., 2015; Haller, 2015), or by searching for the instantaneous fixed points in the velocity field (Conti et al., 2016). The Atlas here employed is based on SSH fields. Hence, first it was necessary to remove the large-scale signals that are irrelevant to capture the mesoscale eddies (with diameters of 100-300 km) by applying a half-power filter cutoff with wavelengths of 20° of longitude by 10° of latitude (Schlax and Chelton, 2016).

In the following lines the process followed to identify the eddies is described in more detail:

(i) For each time, there is a two-dimensional value of SSH $h(i, j)$ with four neighbours. For anticyclonic eddies -concave downward SSH- the identification is made by defining a pixel (i_{ext}, j_{ext}) as a local positive extreme if the SSH values of its four neighbors are less than or equal to $h(i_{ext}, j_{ext})$. Likewise, for cyclonic eddies -concave upward SSH-, a pixel (i_{ext}, j_{ext}) is defined to be a local negative extreme if

the SSH values of its four neighbors are greater than or equal to $h(i_{ext}, j_{ext})$.

(ii) If we assume an anticyclonic eddy with a local maximum SSH at grid location (i_{ext}, j_{ext}) and an indicated threshold SSH value $h_t \leq h(i_{ext}, j_{ext})$, it is possible to define $E(i_{ext}, j_{ext}, h_t)$ as the connected set of pixels (i_l, j_l) , $l = 1, .., n$, which contains (i_{ext}, j_{ext}) and satisfies $h(i_l, j_l) \geq h_t$, $l = 1, ..., n$. Later, some criteria are applied to seek h_b, the minimum value of incrementally decreasing thresholds h_t, such that the compact and coherent structure $E(i_{ext}, j_{ext}, h_b)$, which is an eddy realization with basic SSH value of h_b, satisfies:

1. $n \leq n_{max}$, a determined number of pixels in this structure.
2. $n \geq 2$, a minimum of two interior pixels.
3. Not a single pixel in this structure could have as a neighbor a pixel that belongs to another eddy.
4. The structure is connected. There are not holes on the edges or within the interior of the area.
5. Let $d(i_k, j_k, i_l, j_l)$ be the distance between pixels (i_k, j_k) and (i_l, j_l). So, the maximum value of $d(i_k, j_k, i_l, j_l)$ over all pairs of edge pixels in the structure $E(i_{ext}, j_{ext}, h_t)$ must be less than a specified value d_{max}.

(iii) The set of edge pixels in $E(i_{ext}, j_{ext}, h_b)$ defines the outer perimeter of the eddy realization.

(iv) Eddies are identified by growing sets of pixels from the single pixels at the local maximum in $h(i, j)$ and $-h(i, j)$ for anticyclonic and cyclonic eddies, respectively. This is, given a set of pixels E_l, the next set E_{l+1} is computed by finding all of the neighbors of the edge pixels in E_l that exceed h_{l+1}, which are then added to E_l. At each step E_l, all the criteria above described are checked. If at least one of them is missing, the sequence is stopped. The single pixels at the local maximum are ordered into decreasing size and eddy recognition are obtained from successively smaller initial values of h or $-h$ without attention to polarity.

After the eddy identification, an approximate calculation of different eddy characteristics is computed using the following parameters:

- The eddy centroid coordinates -longitude and latitude (x_c, y_c).
- The amplitude A defined as the difference between the extreme SSH value of $h(i_{ext}, j_{ext})$ and the average of SSH over the edge pixels that define the external perimeter of the eddy.
- The effective radius scale L_{eff} , which is defined to be the radius of a circle with area equal to that of the set of connected pixels $E(i_{ext}, j_{ext}, h_b)$.

- The average of geostrophic speed covering the edge pixels of E_l is found at each threshold $h_l \geq h_n$. The maximum of this average is the rotational or axial speed U of the eddy where, h_U is defined as the threshold SSH at which this maximum average occurs. The speed core of the eddy is then the subset of connected pixels $E(i_{ext}, j_{ext}, h_U)$.

- The speed-based radius scale L, which is defined to be the radius of a circle which area is equal to that enclosed by the contour of maximum circum-average geostrophic speed.

This algorithm was applied on a $1/4° \times 1/4°$ grid using a threshold increment of $\delta = 0.25$ cm and a maximum area $n_{max} = 2000$ pixels. The distance d between the two remotest points must be less than $d_{max} = 400km$ for latitudes greater than $\pm 25°$ and $d_{max} = 700$ km lower than $\pm 25°$ of latitude at the equator, plus an additional restriction of eddies amplitude $A \geq 1$ cm (Schlax and Chelton, 2016).

2.2.2 Eddy tracking

The way to build the path covered by each eddy over time is performing detection on several consecutive days by an automated tracking procedure. An identified eddy has as its center location the geometric center of SSH, as well as the most external and closed contour of SSH. For each eddy identified at time step t, the eddies identified at the next time step $t + 1$ are searched to find the closest eddy lying within an ellipse with zonally oriented major axis where the eastern extreme of the ellipse from the present eddy center is equal to the north-south semi-minor axis of the ellipse (150 km). The distance d of the western extreme is defined according to the increase/decrease of propagation speed related to decreasing/increasing latitude, then, d is set to 1.75 times the distance that a long baroclinic Rossby wave would propagate in one 7-day time step. If the resulting value is less than 150 km, then d is set to 150 km (Chelton et al., 2011b). To conclude, original weekly data was linearly interpolated at a daily basis. This Thesis is based on the daily eddy data.

2.3 Sea Surface Temperature

The Sea Surface Temperature (SST) is a part of the Group for High Resolution Sea Surface Temperature (GHRSST) dataset, which contains daily SST gridded fields with a spatial resolution of $0.25° \times 0.25°$ since 1984. The dataset is produced by interpolating and extrapolating observations from the infrared Advanced Very High Resolution Radiometer (AVHRR) sensors carried on a set of NOAA satellites, and in situ platforms, i.e., ships and buoys (Reynolds et al., 2002). This product is available at: Website GHRSST.

The main drawback of this product is that does not provide reliable measurements when precipitating clouds are present.

2.4 Wind fields

Cross-Calibrated Multi Platforms (CCMP) near-surface global wind fields (U,V) -at 10 m over the sea level- are used in its version 2.0. Winds are provided since 1987 with a spatial resolution of $0.25^\circ \times 0.25^\circ$ every 6 hours and covers almost all Earth (except poles). This product is the result of an optimal merging of different radiometers, scatterometers, buoys and model data using a variational analysis method, and it is available from Remote Sensing Systems (RSS) at: Website RSS.

>

2.5 Spectrum analysis

Power spectral density (PSD), or how the power distributes in a time series within a range of frequencies, is a powerful tool to find frequency patterns of continuous random signals. Thus, significant seasonal, inter-annual or inter-decadal variability can be inferred from a given time series. In this work PSD is computed by using the *periodogram.m* Matlab function, which is based on the Fast Fourier Transform and allows to apply different windows such as the rectangular, Barlett or Welch.

2.6 Coupled Singular Value Decomposition

Singular Value Decomposition (SVD) of two fields (or coupled SVD) allows to extract linear combinations of variables that are likely linearly related. This method is based on the diagonalization of the cross-covariance matrix of both fields (i.e. covariance matrix between their respective grid points). The result is a set of spatially orthonormal patterns and associated time series for each variable (Sayol et al., 2013). The statistical representability (variance explained) of each mode is provided by the eigenvalues of the cross-covariance matrix. Leading modes are usually associated with physical processes, however if this relationship exists (or does not exist) must be demonstrated with additional evidences.

2.7 Self-Organizing-Map

The Kohonen Self-Organizing-Map (SOM), is a powerful unsupervised learning neural network that is often used in pattern recognition, data mining, feature extraction and clustering. By applying the SOM in the spatial domain, we can extract characteristic spatial patterns of the input data matrix. If we transpose the data matrix, and apply the SOM in

the time domain, we can extract characteristic temporal patterns, i.e., the characteristic time series. Since each of these time series represents the temporal variability of a particular region, this method can be used to identify regions of differentiated variability on a map. The SOM, when applied to both space and time domains of the same data, provides a powerful tool for diagnosing ocean processes from such different perspectives. Thus it is called “dual SOM” analysis by Liu et al. (2016).

2.8 Wavelet transform

The continuous wavelet transform allows to extract specific information from time series. In particular, by projecting the time series onto a set of frequency bands the energy corresponding for each band can be inferred. The idea behind this approach is that the original signal can be reconstructed as an appropriate sum of all frequency components. The mother function that is projected by translation (shifting) over each band is known as the mother wavelet. A scaled mother wavelet (a subspace of the original mother wavelet) is known as a child wavelet. Since to obtain all the coefficients in the continuous space is computationally intractable a discrete approach is applied, where an auxiliary function is used (father wavelet) to get the coefficients. The most used set of father and mother wavelets are the Daubechies 4-tap wavelet (Massel, 2001).

Chapter 3

Statistical description of eddy properties

In this section the number of eddies, their location and their fundamental properties (lifetime, amplitude, radius and non-linearity) for the Caribbean Sea region are described statistically. For the sake of clarity, by eddy observations we will refer to each available daily data of a given eddy track, while by eddies we will refer to the statistical average of all observations for each individual mesoscale vortex. In addition, with the aim to identify potential differences in the characteristics of the Caribbean mesoscale eddies from those eddies born in the North-Brazil Current we will separate those initially within the Caribbean Sea from those initially located outside. To this, it has been drawn a polygon that approximately separates the Caribbean Sea from adjacent regions (red polygon in Fig. 3.1), following the natural delimitation imposed by the Greater and Lesser Antilles. According to this division, we have found 1684 (210) eddies inside (outside) the Caribbean Sea between 1993 and 2016 (both years included). The distribution of these initial positions is shown in Fig. 3.1 for all of them (top panel), for only cyclonic (middle panel) and for only anticyclonic eddies (bottom panel) .

3.1 Density of eddies

To better understand the spatial distribution of mesoscale eddies, we have counted the total number of eddy-observations within squared boxes of $0.5^\circ \times 0.5^\circ$ side length in the Caribbean Sea and surroundings (Fig. 3.2). The total number of eddies detected that transit within the Caribbean Sea is 1894 from which 888 (46.8%) are cyclonic and 1006 (53.11%) are anticyclonic. As it is shown in Fig. 3.2 (middle and bottom panels) the spatial distribution of the initial location of anticyclonic and cyclonic eddies is similar and extend over the whole Caribbean Sea, with the exception of the Yucatan Basin and the Colombian Basin (Gulf of Darién) where, although they exhibit a similar pattern, a higher density is presented for anticyclonic eddies. This excess of anticyclonic eddies is consistent with previous studies and partly motivated by the clockwise propagation of the

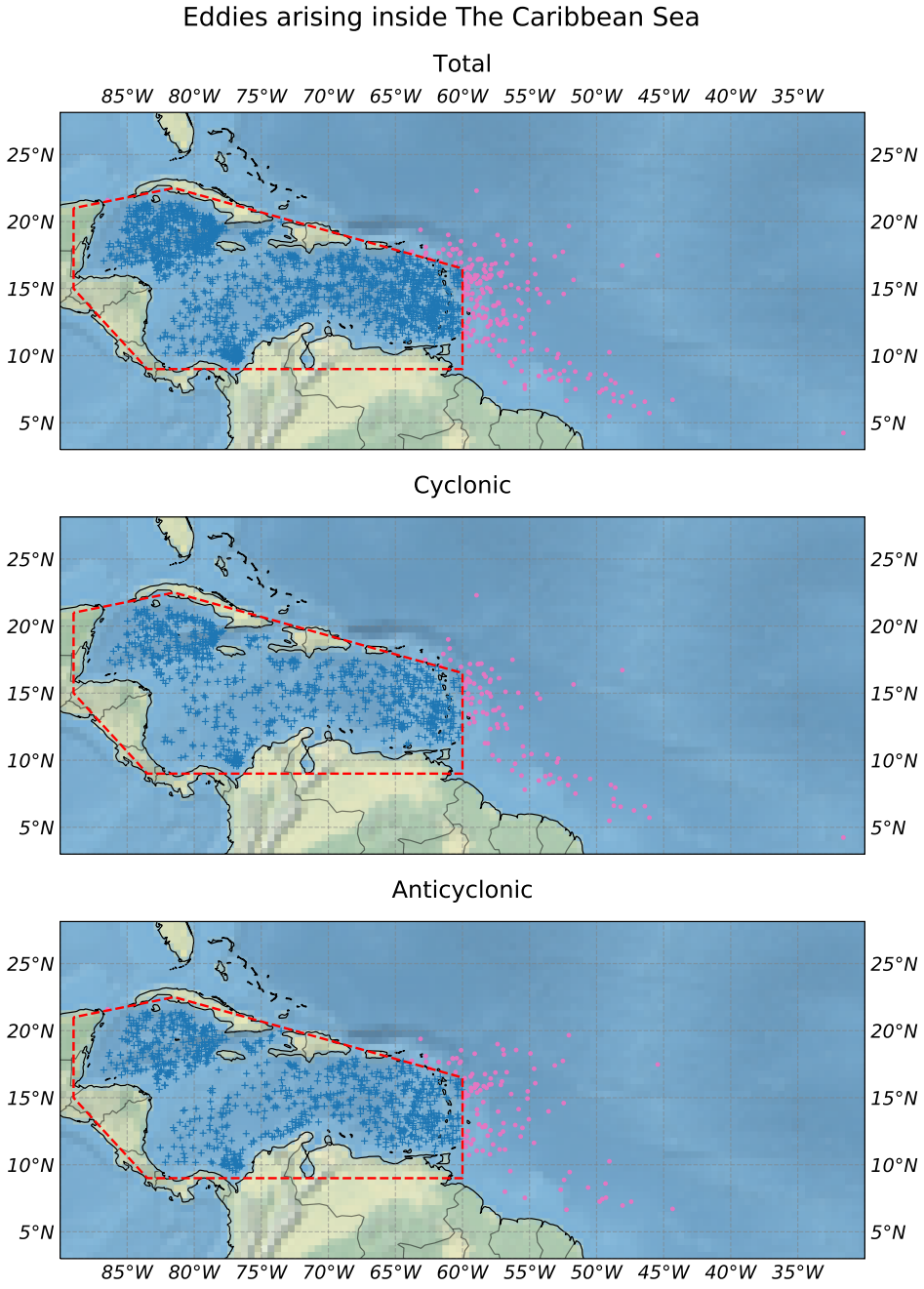

Figure 3.1: Initial location of eddies. The dashed red line denotes approximately the Caribbean Sea. Pink dots indicate eddies outside the Caribbean Sea while dark blue dots indicate eddies within it. Data is presented for all detected eddies (top panel), only cyclonic (middle panel) and only anticyclonic (bottom panel).

western boundary currents along the coasts of the northern part of south America and central America. There eddies become part of, and interact with, the Caribbean Current (e.g. Carton and Chao, 1999; Oey and Lee, 2003). Another reason is that anticyclonic eddies carry out ocean heat content more efficiently from tropical areas to higher latitudes (Rudzin et al., 2017). Jouanno et al. (2008) described permanent features involved in the formation/dissipation of eddies: an anticyclonic recirculation of water in the south of Cuba and a cyclonic gyre (Panama-Colombia Gyre) characterized by the episodic formation of cyclonic eddies that quickly dissipate when interact to the southern Caribbean anticyclones.

3.2 Eddy properties

In this section the following properties of Caribbean Sea eddies are statistically described: lifetime, amplitude, radius and degree of non-linearity (which indeed includes information on the rotational speed and on the translation speed of eddies).

Histograms of those eddies properties with at least one observation within the Caribbean Sea are shown in Fig. 3.3. The mean and the standard deviation are indicated by μ and σ respectively. Results are provided for the 888 cyclonic and 1006 anticyclonic eddies. The main results for each parameter are summarized below and in Table 1:

Lifetime: The average lifetime for the whole set of eddies is 68.0 ± 45.0 days (mean $\pm$ standard deviation), and 69.9 ± 48.2 days for cyclones and 66.3 ± 41.9 days for anticyclones eddies with the longest-lived anticyclonic and cyclonic eddies lasting 319 days and 290 days respectively (Fig. 3.3a-c). A vast majority of mesoscale eddies ($> 85\%$) have a lifetime shorter than 120 days.

Amplitude: The amplitude of eddies, which was defined in section (2.2.1), is shown in Fig. 3.3d-f. The mean value of A is 6.8 ± 3.6 cm for cyclonic (Fig. 3.3e) and 7.9 ± 4.2 cm for anticyclonic eddies (Fig. 3.3f). This result is congruent with Gaube (2013), who found that the eddy field of the Caribbean Sea is characterized by mesoscale eddies with average amplitudes of 7.8 cm, as well as with the latitudinal variation of the zonally averaged eddy amplitude found by Chelton et al. (2011b). However, Chelton et al. (2011b) pointed out that the predominance of small eddy amplitudes may raise concerns that the distribution of observed eddy amplitudes is influenced by the procedure applied in their work, which may sometimes be biased low by 1 or 2 cm in regions of very energetic mesoscale variability and by less than 1 cm in less energetic regions due to the complex geometry of many eddies.

Radius: There are no significant differences between both eddy polarities in the effective radius scale, which also has been defined in section 2.2.1. Radii range from 50 to 250 km, as expected from the spatial resolution of the employed altimetric product. The mean radius is 105.0 ± 30.0 km for cyclonic and 97.5 ± 28.3 km for anticyclonic

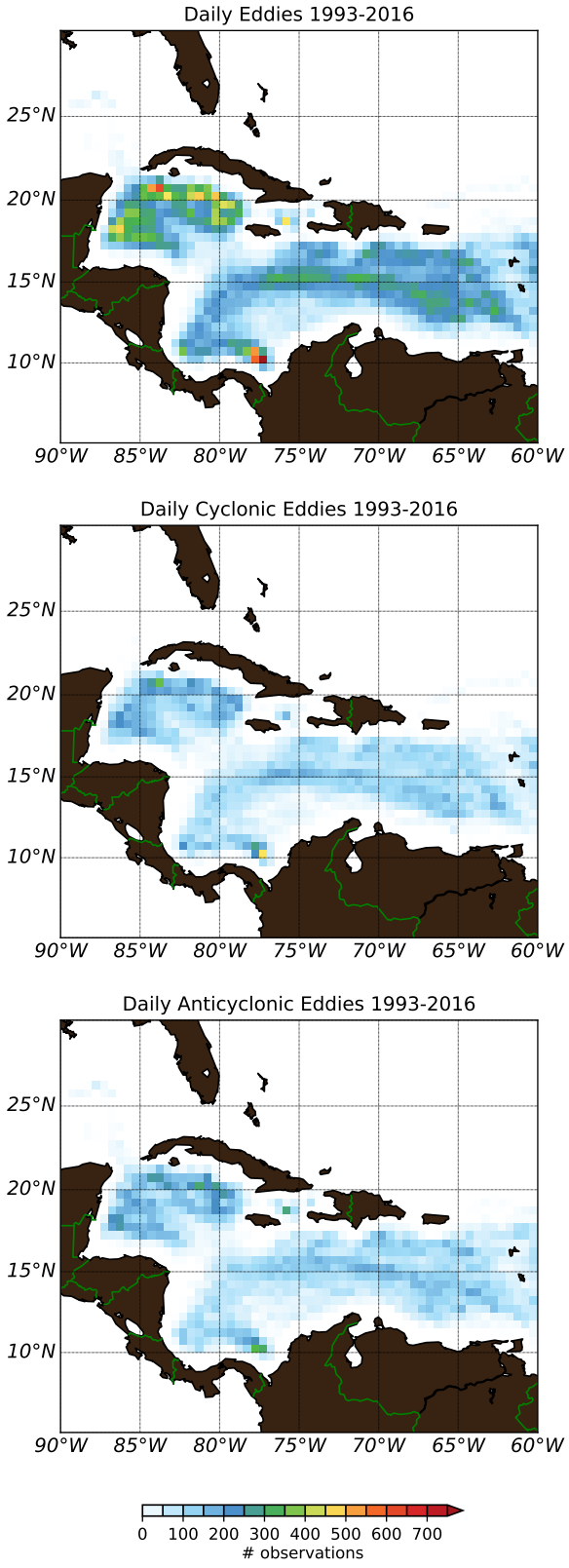

Figure 3.2: Number of eddy-observations from January 1^{st} 1993 to December 31^{st} 2016 within boxes of $0.5° \times 0.5°$ side length. It includes all observations (top panel), only cyclonic observations (middle panel) and only anticyclonic observations (bottom panel).

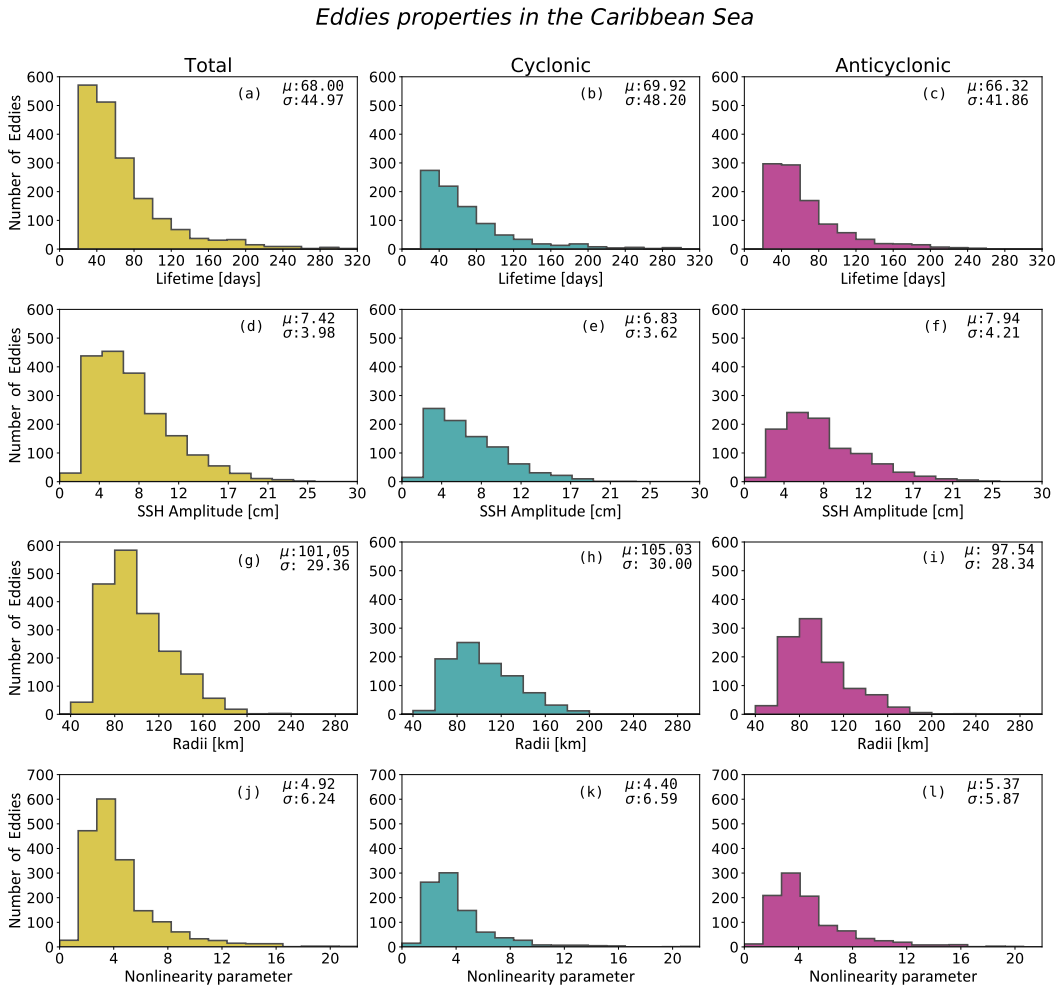

Figure 3.3: Histograms of properties of Caribbean Sea eddies from January 1993 to December 2016. First row: lifetime for all eddies a), only cyclonic b) and only anticyclonic c). Second row: Histogram of time-mean amplitude for all eddies d), only cyclonic e) and only anticyclonic f). Third row: Histogram of time-mean radius for all eddies g), only cyclonic h), only anticyclonic i). Bottom row: histogram of the time-mean non-linearity parameter for all eddies j), only cyclonic k) and only anticyclonic l). The non-linearity parameter is defined as the rotational velocity divided by the translational speed.

eddies (Fig. 3.3h-i). This result is consistent with the latitudinal distribution of eddy sizes described by Chelton et al. (2011b) where eddies of around 200 km of radii are found in the near-equatorial regions to later monotonically decrease up to 80 km at 20° of latitude. We note that these length-scales of eddies and eddy-like features are constrained by the Rossby radius of deformation.

Non-linearity: The parameter of non-linearity is defined as U/c, where U is the rotational speed of each eddy and c is the translational speed. A value of $U/c \geq 1$ implies that the mesoscale eddy cannot be regarded as a linear wave disturbance propagating through a nearly stationary medium, but instead is capable of modifying the medium by advecting a trapped fluid parcel as it translates (Chelton et al., 2011b), transporting water properties such as heat and salt, as well as biogeochemical characteristics such as nutrients and phytoplankton. Fig. 3.3j-l shows the histograms of the parameter of non-linearity averaged for each eddy indicating that, all combined, cyclonic and anticyclonic eddies are non-linear (Fig. 3.3(j-l), with over 80% of eddies showing $U/c \geq 1$. Indeed, over 21% of cyclonic and 33$\%$ of anticyclonic eddies are highly nonlinear with $U/c > 5$ and few, 3% cyclones and 6% anticyclones, are strongly non-linear ($U/c > 5$). These values of U/c are in good agreement with the results that can be inferred from Chelton et al. (2011b) in the Caribbean Sea region.

Normalized eddy properties

To examine the general patterns in the eddy properties we have proceeded to normalize the amplitude, radii and non-linearity of eddies according to their lifetime. To this, for each eddy track, the first value of lifetime is considered the *birth* (normalized lifetime of 0) and the last value the *death* (normalized lifetime of 1) of the eddy. Subsequently the lifetime of each eddy has been divided in regular subperiods of 0.01 from 0 and 1. Later, the mean value of each parameter within each subperiod has been computed and scaled with respect to the first value at birth, which provides a normalized value of 1 for each eddy and for all properties at the initial time. Finally, all eddy-observations within the corresponding subperiod have been averaged. As a result, a general curve showing the evolution of each eddy property for all eddy observations for a normalized lifetime is obtained.

Results indicate that eddies tend to increase substantially in amplitude and radii during the first part of their life (around 90% in amplitude and 35% in radii) reaching the maximum development at around the middle of their lifetime (Fig. 3.4 upper and middle panel). Once eddies have reached their maximum amplitude they tend to spend another 25% of their lifetime with the same amplitude, to later start a fast decay till reaching again the initial values at the end of their lifetime. A similar process occurs with the radii, although in this case anticyclonic eddies are able to stabilize their radii better than cyclonic eddies, for which their radii is constantly changing. Besides, other differences between the behaviour of anticyclonic and cyclonic eddies worthy to point out are that anticyclonic

eddies increase slightly more their amplitude than cyclones (Fig. 3.4 upper panel), and that cyclonic eddies reach their maximum radii a bit later that anticyclonic eddies with a delay of around 10% in the normalized lifetime (Fig. 3.4 middle panel). These results suggest that the lifetime of an eddy may be predicted once the peak of the amplitude has been reached, which would be different from the statement of Chelton et al. (2011b), who argued that the amplitude of an eddy is not enough to determine its longevity.

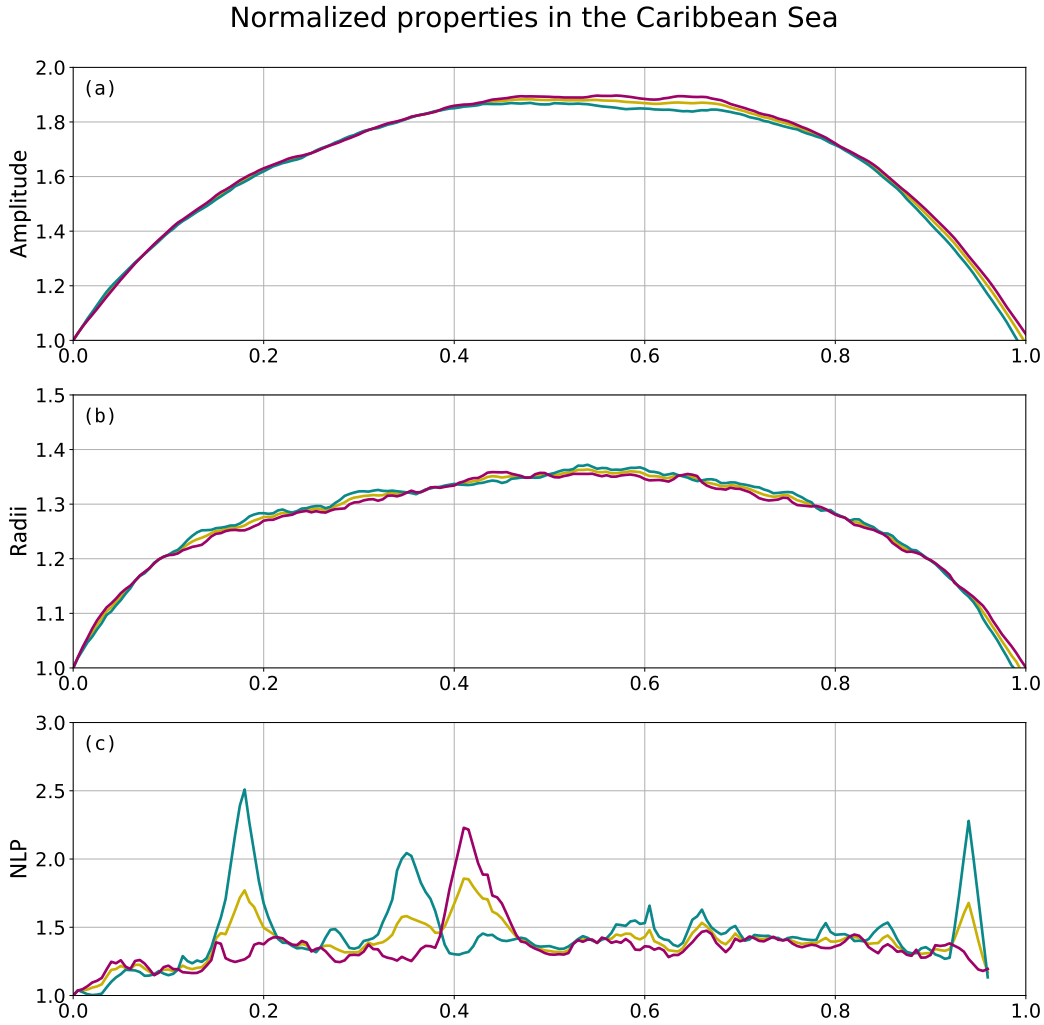

Figure 3.4: Mean properties of eddies normalized by their lifetime and scaled by their initial value. First row: Eddy amplitude of all eddies (yellow line), only cyclonic (blue line) and only anticyclonic (pink line). Second row: eddy radii of all eddies (yellow line), only cyclonic (blue line) and only anticyclonic (pink line). Third row: non-linearity of all eddies (yellow line), only cyclonic (blue line) and only anticyclonic (pink line).

Contrarily, the plot of the normalized parameter of non-linearity with respect to the normalized lifetime (Fig. 3.4 bottom panel) shows significant differences according to the polarity of eddies. Thus, overall cyclonic eddies tend to be more non-linear and unstable that anticyclonic eddies during their lifetime. Specially remarkable is the abrupt peak towards the end of the lifetime of cyclonic eddies which is suggested to be a potential indicator of the end of their life. Contrarily, anticyclonic eddies dissipate after a short and

smooth decay in their value of non-linearity.

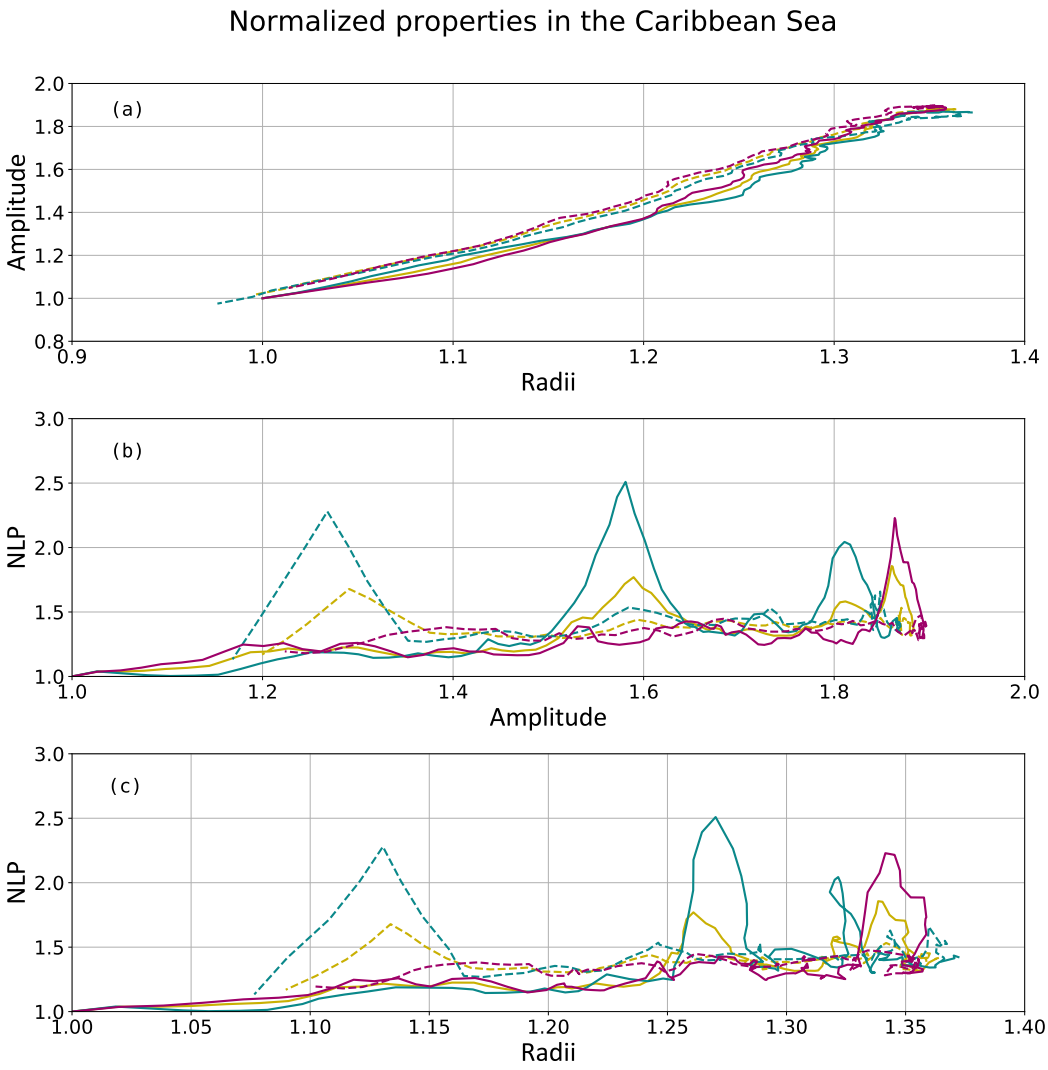

Figure 3.5: Life-cycle of pairs of eddy properties based on Fig. 3.3. Upper panel: normalized eddy radii vs normalized eddy amplitude of all (yellow line), only cyclonic (blue line) and only anticyclonic (pink line) eddies. Middle panel: normalized eddy amplitude vs normalized parameter of non-linearity for all eddies (yellow line), only cyclonic (blue line), and only anticyclonic eddies (pink line). Lower panel: normalized eddy radii vs normalized parameter of non-linearity for all (yellow line), only cyclonic (blue line), and only anticyclonic (pink line) eddies. Solid and dashed lines indicate the first and second half of normalized lifetime respectively.

A plot showing the mean co-evolution of the normalized properties of Fig. 3.4 is shown in Fig. 3.5. On average, Caribbean Sea eddies grow in amplitude and radii until half of their lifetime (0.54 of their their scaled lifetime), growing 36% in radii and 88% in amplitude (Figures 3.5 upper and middle panel. From that moment the eddies decrease almost linearly both in amplitude and in radius. Contrarily, the parameter of non-linearity does not show a clear relationship with eddy amplitude and radii (Fig. 3.5 bottom panel).

3.3 Trajectories of mesoscale eddies

In addition to the characterization of the fundamental properties of eddies, we have drawn their trajectories. The objective is to visualize the main areas of eddy formation and the preferred eddy pathways. Also we are interested in knowing their areas of dissipation and if any differences arise between cyclonic and anticyclonic eddies, as well as the seasonal variations of their trajectories. Fig. 3.1 shows that most of eddies form in the eastern Caribbean Sea or are already formed in the north east of Brazil, some off the Colombian coast, and the reminder in the Cayman and Yucatan Basin. Fig. 3.6 shows all eddies with mean westward (blue lines) and eastward (pink lines) propagation (upper panel), also distinguished their polarity (cyclonic in the middle panel and anticyclonic eddies in the bottom panel). The dominant direction of propagation is westward due to the dominant boundary current with 816 cyclonic and 897 anticyclonic eddies, while those eddies that propagate eastward represent a smaller portion: 109 anticyclonic and 72 cyclonic eddies. A seasonal assessment according to the mean direction of eddies is presented below:

- *Westward direction.* The seasonal trajectory for eddies propagating westward shows that 627 eddies arise during the dry season with 51.2% of them being anticyclonic, and no clear differences in the spatial distribution of eddies with both polarities (Fig. 3.7a-c). Throughout the transitional season (Fig. 3.7d-f), the spatial distribution looks different for the Colombia Basin with a total number of eddies of 297 (54.54% are anticyclones). The difference in the spatial distribution for cyclonic (49%) and anticyclonic (51%) eddies holds for the Veranillo de San Juan season (Fig. 3.7g-i). In this case more eddies form at the eastern side, while less cyclonic eddies form off the Colombian basin. During the wet season more eddies develop in the Colombian Basin with a total number of 383, of which 46% are cyclonic and 54% anticyclonic eddies (Fig. 3.7j-l).

- *Eastward direction.* In this case there are significant differences in both eddy polarities during the dry (Fig. 3.7b-c) and Veranillo de San Juan (Fig. 3.7h-i) seasons. The dry season is characterized by less cyclonic than anticyclonic eddies in the Yucatan Basin, while the opposite occurs in the northwestern Colombian basin. In total, the number of eddies in this season with eastward propagation are 72, of which 59% are anticyclonic. The differences in Veranillo de San Juan season are in the Colombian Basin and in the southern part of Venezuela Basin where there are more anticyclonic eddies. This season has a total of 37 eddies of which 76% are anticyclonic.

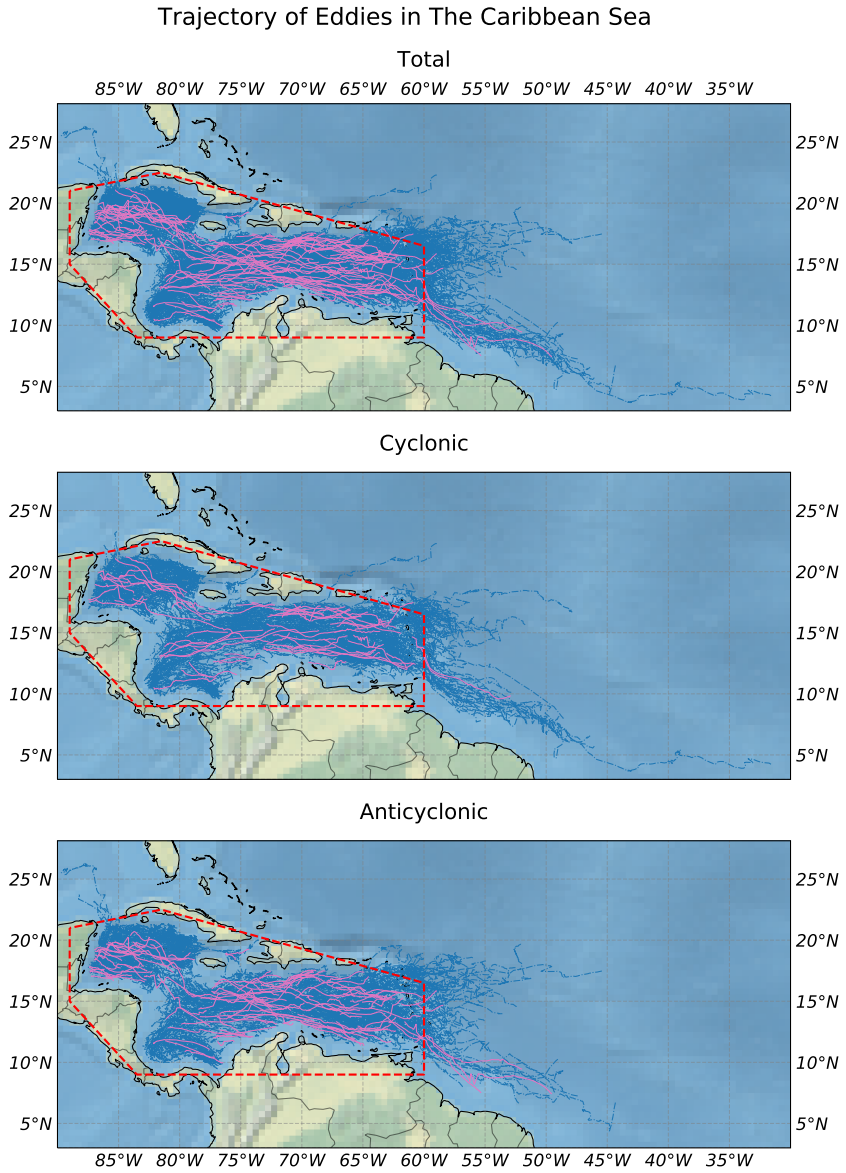

Figure 3.6: Trajectories of detected Caribbean Sea eddies between 1993 and 2016 from the Eddy Aviso atlas. The dashed red line indicates the area of study. Pink lines indicate all eddies with eastward propagation while blue lines indicate those eddies moving westward inside the domain for both polarities (upper panel), only cyclonic (middle panel) and only anticyclonic eddies (bottom panel)

Table 3.1: Properties of detected eddies averaged according to season and propagation (West-East) from January 1993 to December 2016 for all eddies, cyclonic and anticyclonic.

Eddies in the Caribbean Sea									
	Eddy property	**Dry**		**Transition**		**Veranillo de San Juan**		**Wet**	
		West	East	West	East	West	East	West	East
Total	N = 1894	627	72	297	30	406	37	383	42
	Lifetime [day]	66.0 ± 40.6	42.9 ± 17.7	76.8 ± 50.7	49.8 ± 23.2	75.1 ± 51.1	50.9 ± 29.5	67.2 ± 44.6	44.6 ± 17.6
	Amplitude [cm]	6.8 ± 3.5	7.3 ± 4.8	7.9 ± 4.1	7.0 ± 4.1	7.9 ± 4.2	9.6 ± 5.9	7.4 ± 3.9	7.2 ± 3.9
	Radius [km]	98.9 ± 28.2	97.6 ± 31.5	101.2 ± 28.7	96.3 ± 25.2	105.0 ± 30.3	113.4 ± 35.7	101.0 ± 29.8	92.8 ± 24.5
	Rot. vel. [cm/s]	28.3 ± 8.5	30.3 ± 10.0	30.9 ± 9.7	30.4 ± 8.8	31.0 ± 9.4	35.2 ± 12.5	29.8 ± 9.2	30.1 ± 7.4
	Trans. vel. [cm/s]	14.1 ± 5.4	12.8 ± 3.6	13.6 ± 4.8	13.4 ± 4.0	13.1 ± 4.7	13.1 ± 3.3	13.5 ± 4.7	12.9 ± 3.5
	Non-linearity	4.9 ± 8.2	3.3 ± 2.1	4.9 ± 3.9	3.6 ± 2.7	5.4 ± 4.8	3.5 ± 1.7	5.0 ± 6.7	3.3 ± 1.1
Cyclonic	N = 888	306	30	135	14	198	9	177	19
	Lifetime [day]	68.5 ±46.0	48.8 ± 23.4	77.4 ± 50.0	43.6 ± 17.5	74.1 ± 53.9	45.7 ± 34.2	71.7 ± 48.8	44.7 ± 16.2
	Amplitude [cm]	6.5 ± 3.4	7.1 ± 4.4	7.6 ± 3.9	6.6 ± 3.9	7.1 ± 3.7	8.1 ± 4.9	6.7 ± 3.4	5.3 ± 1.8
	Radius [km]	103.4 ± 31.1	113.1 ± 38.9	106.0 ± 29.7	101.8 ± 26.4	107.6 ± 27.2	114.0 ± 46.2	104.4 ± 29.3	88.5 ± 19.7
	Rot. vel. [cm/s]	26.7 ± 8.2	29.5 ± 9.7	29.3 ± 8.5	27.8 ± 8.3	28.9 ± 8.6	30.9 ± 8.1	27.8 ± 8.0	26.5 ± 4.6
	Trans. vel. [cm/s]	14.4 ± 5.3	13.2 ± 3.2	13.6 ± 4.5	14.5 ± 3.6	13.9 ± 4.9	12.8 ± 2.8	14.1 ± 4.7	12.9 ± 3.5
	Non-linearity	4.8 ± 10.7	2.9 ± 1.3	4.4 ± 2.7	2.7 ± 0.9	4.5 ± 2.8	3.0 ± 0.9	4.2 ± 2.4	2.9 ± 1.7
Anticyclonic	N = 1006	321	42	162	16	208	28	206	23
	Lifetime [day]	63.7 ± 34.6	38.6 ± 10.7	75.4 ± 51.4	55.1 ± 26.7	76.1 ± 48.3	52.5 ± 28.4	63.4 ± 40.5	44.6 ± 18.9
	Amplitude [cm]	7.2 ± 3.6	7.3 ± 4.2	8.2 ± 4.3	7.3 ± 4.3	8.7 ± 4.4	10.1 ± 6.2	7.9 ± 4.2	8.7 ± 4.5
	Radius [km]	94.6 ± 24.5	86.6 ± 18.4	97.1 ± 27.3	91.6 ± 23.9	102.5 ± 32.7	113.2 ± 32.7	98.1 ± 30.0	96.3 ± 27.8
	Rot. vel. [cm/s]	29.7 ± 8.5	30.9 ± 10.3	32.5 ± 10.4	32.6 ± 8.8	32.9 ± 9.6	36.6 ± 13.4	31.4 ± 9.8	33.1 ± 7.9
	Trans. vel. [cm/s]	13.8 ± 5.5	12.5 ± 3.8	13.6 ± 5.1	12.5 ± 4.3	12.3 ± 4.4	13.2 ± 3.5	13.0 ± 4.6	12.9 ± 3.6
	Non-linearity	5.2 ± 4.7	3.6 ± 2.4	5.5 ± 4.6	4.4 ± 3.5	6.2 ± 5.9	3.6 ± 1.8	5.7 ± 8.7	3.6 ± 1.1

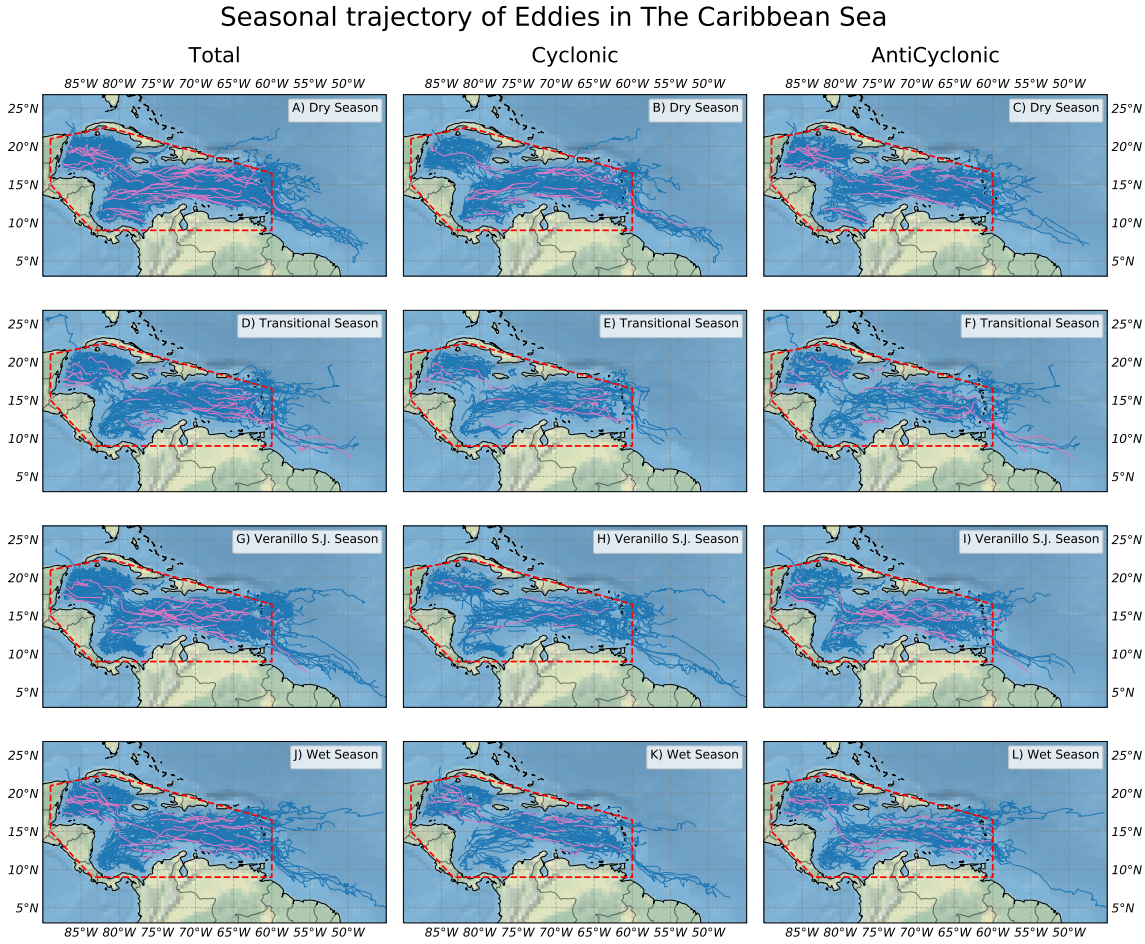

Figure 3.7: Trajectories of eddies separated by the season of their initial value. The dashed red line indicates the area of study. Pink lines indicate eastward propagation while blue lines indicate westward propagation in upper row: Dry season for a) All eddies, b) cyclonic and c) anticyclonic eddies. Second row: Transitional Season for: d) all eddies, e) cyclonic and f) anticyclonic eddies. Third row: Veranillo de San Juan Season for g) all eddies, h) cyclonic and i) anticyclonic eddies. Lower row: Wet season for j) all eddies, k) cyclonic and l) anticyclonic eddies.

To conclude this part on eddy trajectories histograms of the traveled distance by eddies in the Caribbean Sea are shown in Fig. 3.9 for all eddies (top row) and for eddies moving westward (middle row) and eastward (bottom row). On average eddies tend to travel more than 500 km, but it depends strongly on the considered eddy (σ). The mean distance is especially larger for those cyclonic eddies moving westward, but also the dispersion of values is larger for these eddies. A small percentage of eddies ($< 20\%$) travel more than 750 km with few of them covering a distance over 2000 km. These eddies are those that move along the southern/southwestern Caribbean Sea following the boundary current.

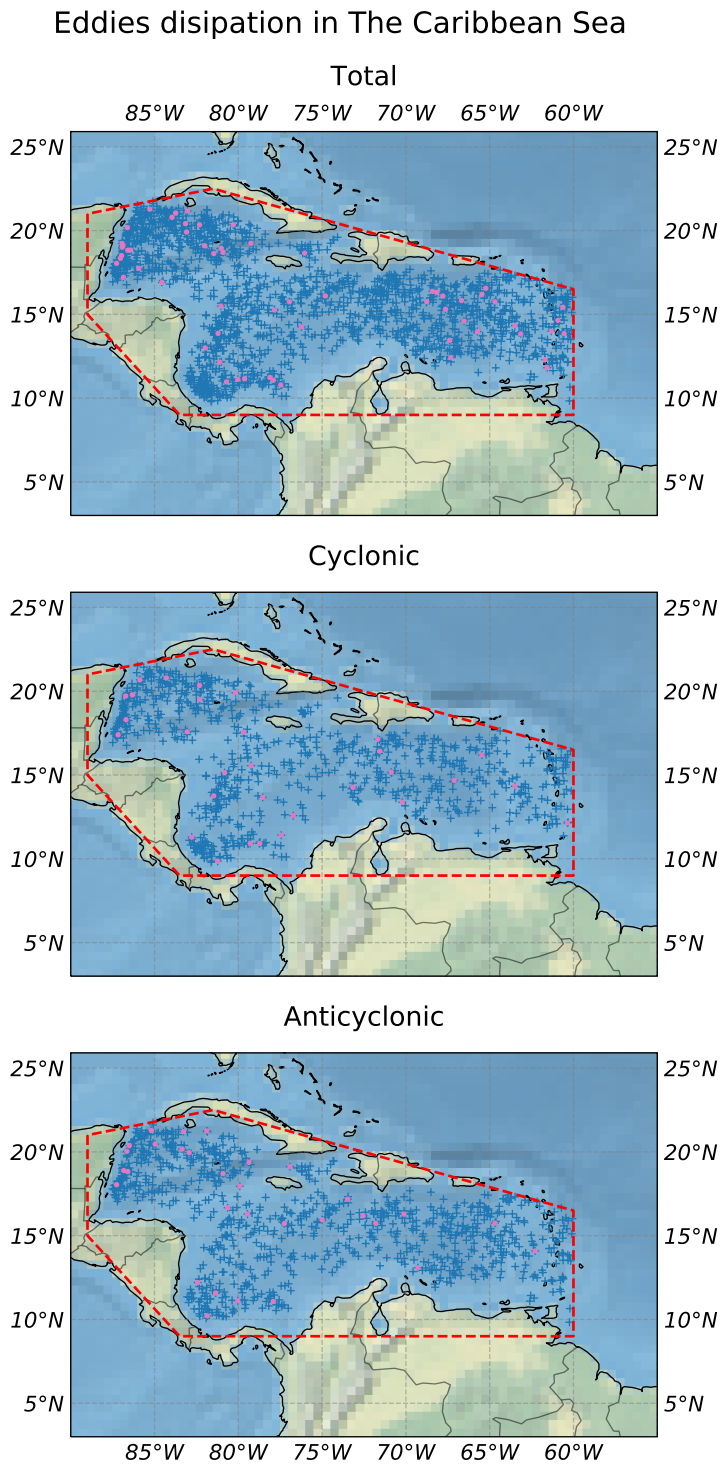

Figure 3.8: Final location of eddies. The dashed red line denotes approximately the area covered by the Caribbean Sea. Pink dots indicate those eddies that started outside the domain while dark blue dots indicate eddies starting and ended within the Caribbean Sea. Data is presented for all (top panel), only cyclonic eddies (middle panel) and only anticyclonic eddies (bottom panel).

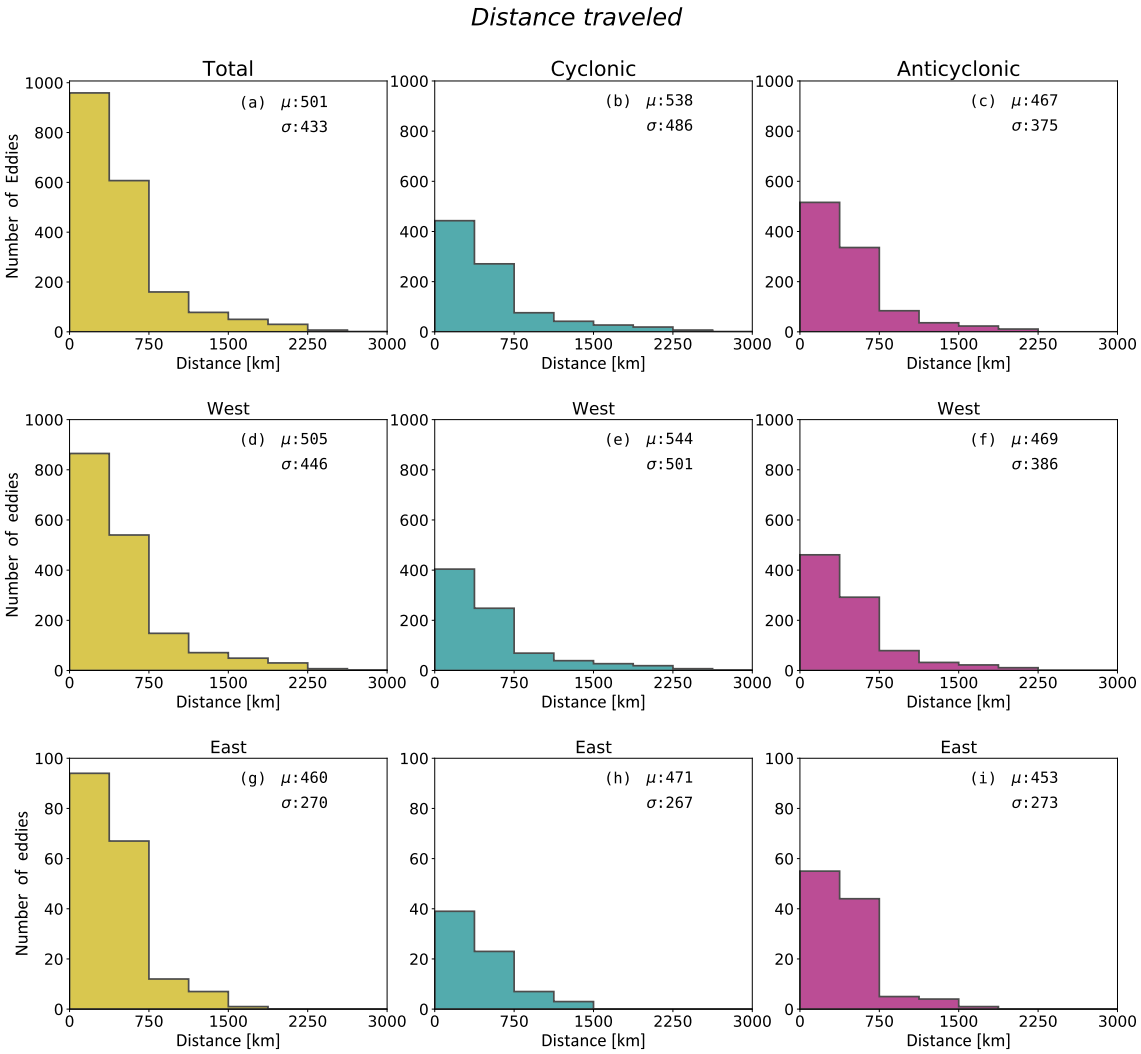

Figure 3.9: Histograms of distance traveled by eddies. First row: Distance traveled for all (a), only cyclonic (b) and only anticyclonic eddies (c). Second row: Histogram of the westward distance traveled for all eddies (d), only cyclonic (e) and only anticyclonic (f). Third row: Histogram of eastward distance traveled for all eddies (g), only cyclonic (h), only anticyclonic (i).

Chapter 4

Seasonal and inter-annual variability in the distribution of eddies

In this Chapter first the relationship between the number of eddy observations and both, the sea surface temperature (SST) and the surface wind is assessed at seasonal scale. Later, the connection between the inter-annual variability of the number of eddy-observations and the ENSO phenomenon is also evaluated.

4.1 Seasonal variability

The Caribbean Current is the major route by which South Atlantic waters flow into the Florida Current to join the Gulf Stream being therefore a key passage of the upper part of the Atlantic Meridional Overturning Circulation (AMOC). It is well known that this circulation makes the largest oceanic contribution to the meridional redistribution of heat in the Caribbean Basin. The AMOC at sub-tropical latitudes presents an inter-annual variability that fluctuates around 4.8 Sv and a seasonal cycle of around 6.7 Sv with its maximum strength in autumn and its minimum in spring (Kanzow et al., 2010). This seasonality in the AMOC was commonly thought to be dominated by the northward Ekman transport thus reflecting the particular relevance of wind field in the ocean dynamics of Caribbean Sea.

Spectrum analysis is concerned with the exploration of periodicities in time series. The purpose of the analysis is to decompose a complex time series with cyclical components into few dominant underlying sinusoidal (sine and cosine) functions of particular wavelengths.

First, it is investigated the dominant-scale that may explain the temporal variability in the daily and monthly number of eddy-obervations. To this end it is applied a spec-

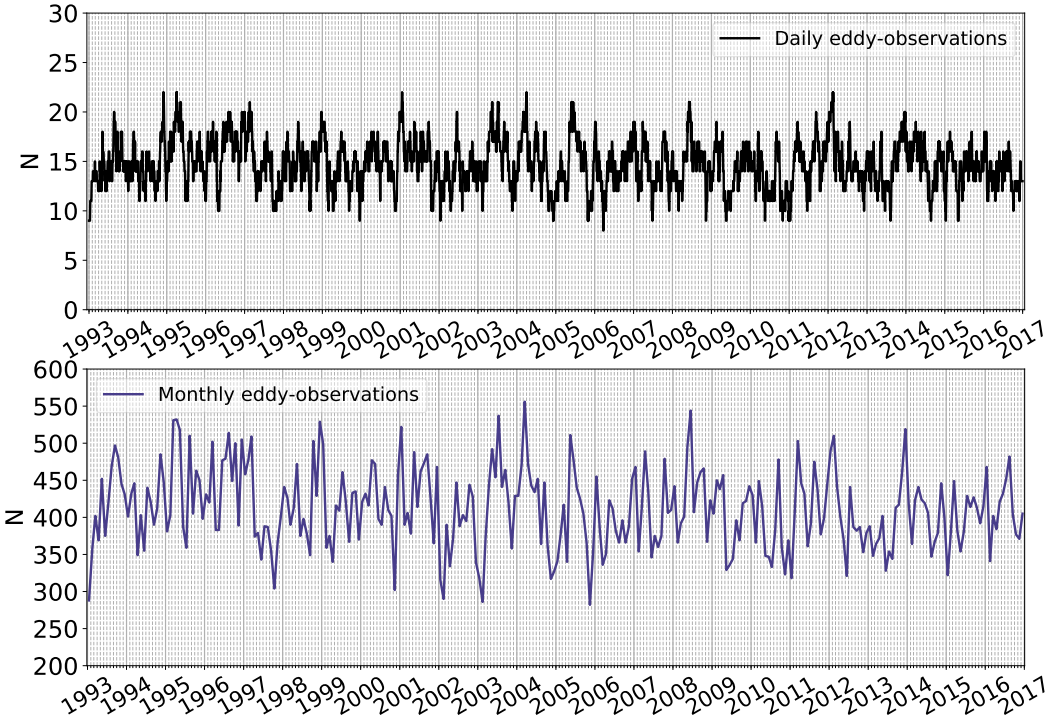

Figure 4.1: Time series of eddy-observations from 1993 to 2016 in the Caribbean Sea at daily (top) and monthly (bottom) time scales.

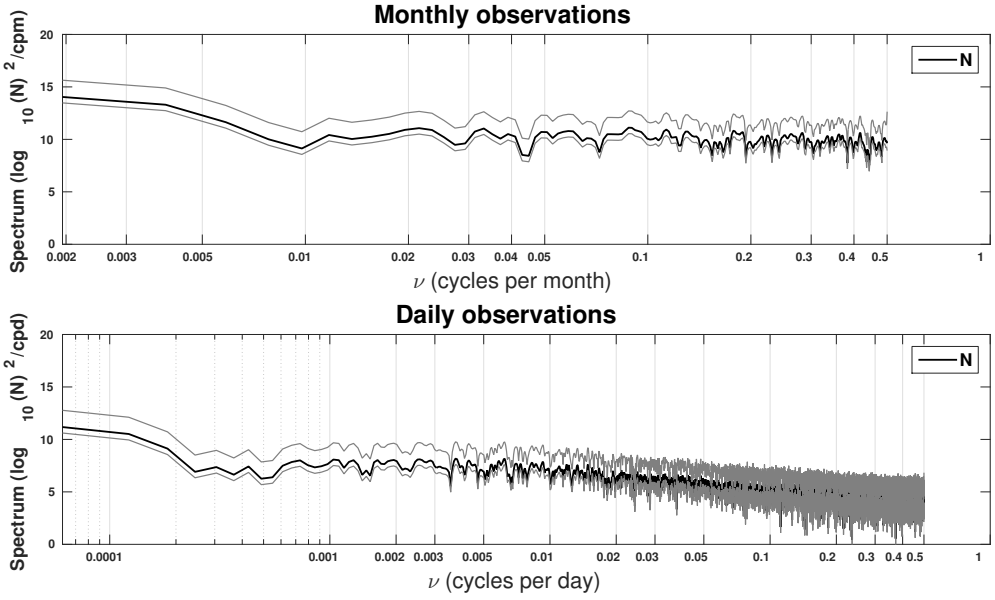

Figure 4.2: Top: Fast Fourier Transform (FFT) spectra for the monthly eddy-observations. Bottom: FFT spectra for the daily eddy observations. Black line correspond to observations and gray to the 5 and 95% confidence levels.

tral analysis based on the Fast Fourier Transform (FFT) [1]. The time series analyzed are the accumulated number of daily and monthly eddy-observations over the region from 1993 to 2016 (see Fig. 4.1). Fig. 4.2 shows the monthly (top panel) and daily (bottom panel) spectra for the number of eddy-observations in which the black line corresponds to spectrum and the gray lines denote the 5% and 95% confidence levels. Although some periodicity can be inferred between 5 and 12 months (around 0.2 and 0.08 cycles per month), peaks are not sufficiently clear to be conclusive about the existence of any cycle in the signal. The same conclusion is obtained using the time series of daily observations, in which the spectrum is even noisier.

Regarding the periodicity for separated cyclonic and anticyclonic observations (Fig. 4.3, top and bottom respectively), results are also not conclusive although for anticyclonic eddies some kind of periodicity around 40-50 months (0.02-0.025 cycles per month) is hardly observed (bottom panel). Despite the absence of a clear seasonal signal in the spectrum when it is considered the number of eddies in the whole basin, it is still possible that some seasonality exists in certain specific Caribbean Sea regions. To bring more light on this possibility, the potential link between the spatial distribution of eddy-observations and key variables with strong seasonality such as the SST or the surface wind is evaluated in the following sections.

4.1.1 SST and eddy observations density coupled SVD analysis

Many processes are known to influence the distribution of SST such as the direct radiative forcing or the wind-induced mass transport. In this section the relation between the spatio-temporal distribution of eddy-observations and the AVHRR-based SST time series in the Caribbean Sea is evaluated. To do this it has been applied a coupled SVD analysis between SST and the number of eddy-observations (see Section 2.6 for more details on this method).

At each grid point both variables have been linearly detrended and normalized (mean subtracted and divided by the typical deviation). As a result, now we have fields of SST and eddy-observations anomalies. The first spatial pattern of covariability (referred as a mode) between eddy-observations (top-left) and SST (top-right) for the Caribbean Sea is shown in Fig. 4.4. This pattern explains the largest part of the covariance of both signals with a 92.6% of the total. Temporal amplitudes for both variables are shown in Fig. 4.4 (middle panel, black line for the monthly distribution of the number of eddies and purple for SST). Clearly, both signals are negatively correlated with a periodicity of 12 months (bottom panel). A point to note is that the spatial pattern of SST anomalies is

[1] The standard (and most efficient) FFT algorithm requires that the length of the input series is equal to a power of 2. If this is not the case, additional computations have to be performed. For long time series, in order to still utilize the FFT algorithm, an implementation of the general approach described by Monro and Branch (1977) is used. This method requires significantly more storage space, although series of considerable length can still be analyzed very quickly, even if the number of observations is not equal to a power of 2

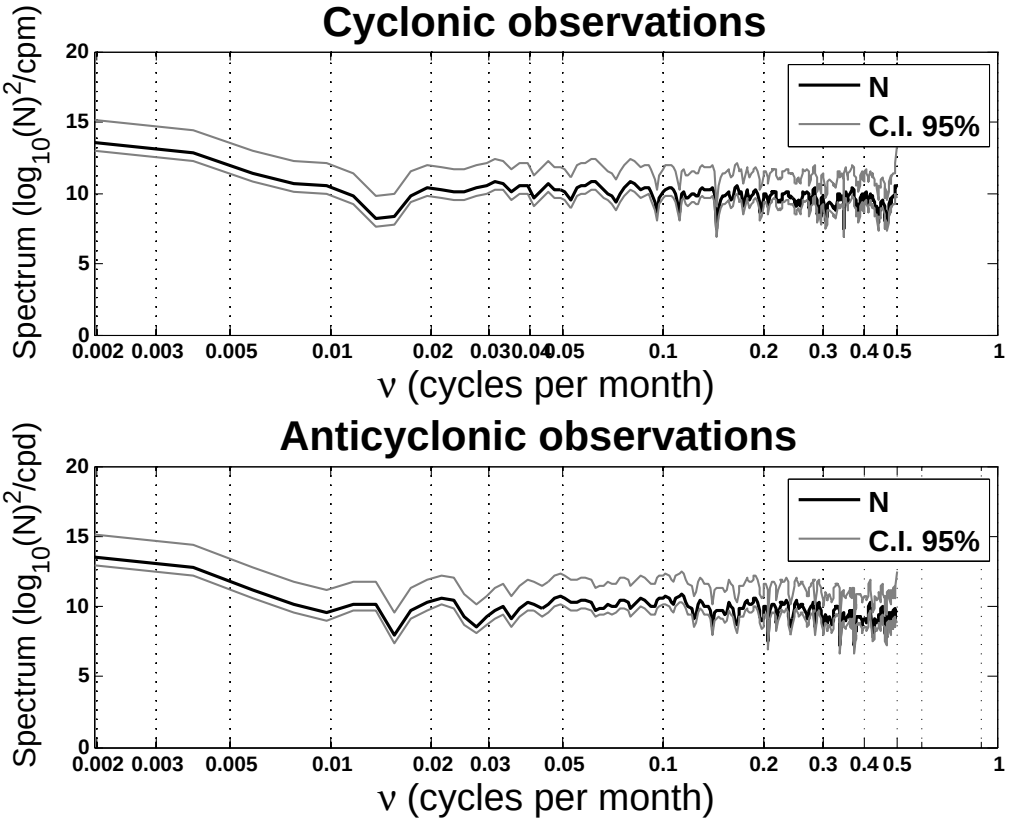

Figure 4.3: Fast Fourier Transform (FFT) spectra for the number total monthly cyclonic eddy-observations (top), and for the monthly anticyclonic eddy-observations (bottom). The black line corresponds to the mean spectrum whereas gray lines denote the 5 and 95% confidence levels.

positive for the whole basin; it means that when the amplitude is positive, the SST field yield values above the mean, while the opposite occurs when the amplitude is negative. As expected, SST increases during the second half of the year (Veranillo de San Juan and dry seasons). Conversely, the number of eddy-observations follows a more complex pattern as it increases or decreases depending on the location of the considered basin (Fig. 4.4, top left), but a notably seasonal cycle appears (black line in middle panel). As observed, around the Colombian and Venezuelan basins, the mode shows values of eddy-observations above the mean. Thus, when the SST is above the mean, the number of observations decreases since the temporal amplitude is negative. The opposite happens in those areas with blue shading such as near the Yucatan Chanel or in the mid-western Caribbean Sea, which shows more eddy-observations during summer.

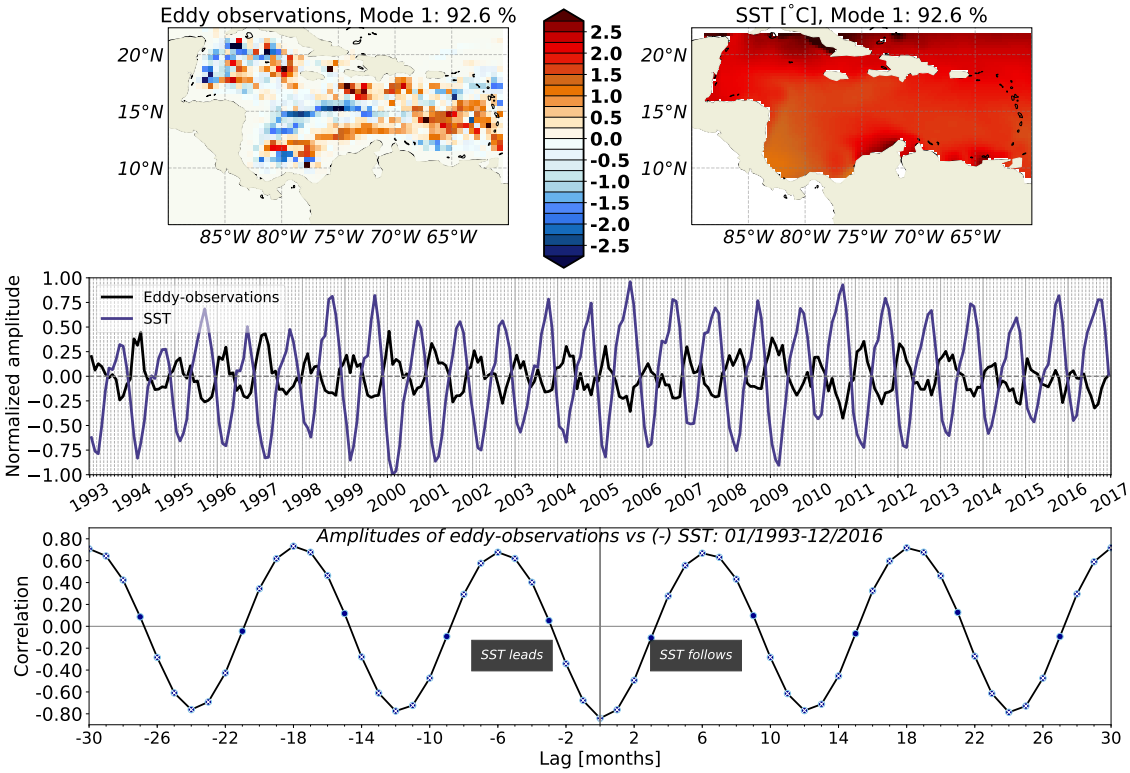

Figure 4.4: Top: First coupled SVD spatial mode for the distribution of the anomalies of eddy-observations (left) and for the anomalies of SST (right). Middle: Corresponding temporal amplitude for eddy-observations (black) and for the SST (purple). Bottom: Cross-correlation between both temporal amplitudes shown in the middle panel.

4.1.2 Wind curl and density of eddy-observations coupled SVD analysis

The importance of the surface wind in the formation (and/or destruction) of basin-scale vortexes has already been shown by several authors (e.g. Moskalenko, 1974; Malanotte-Rizzoli and Bergamasco, 1989, 1991; Herbaut et al., 1996; Pinardi and Navarra, 1993). Molcard et al. (2002) shown that the wind forcing can generate upper ocean gyres with observable structure and strength. As the wind forces the coastal circulation, the interaction between the wind and the coastal topography, such as headlands and capes, may have a strong effect on shallow water hydrodynamics (e.g. Castelao and Barth, 2006, 2007). In particular, topographically-induced changes in wind speed and in wind stress curl are usually associated with flow variability, formation and growth of instabilities around promontories. Moreover, the coastal circulation is highly influenced by the shape of the coastline. Leeward eddies are observed behind topographic structures like prominent headlands and capes (e.g. Pattiaratchi et al., 1986; Farmer et al., 2002; McCabe et al., 2006). From a dynamical point of view, capes and headlands are important for the circulation because they are associated with enhanced mixing, drag and dissipation (Farmer et al., 2002; Pawlak et al., 2003). All processes usually observed around capes, like current separation, formation of eddies and generation of lee waves, also affect the larger-scale coastal currents through the enhancement of the drag force. Altogether, the combination of a cyclonic (positive) wind curl and easterly winds can generate opposite alongshore currents in the southern Caribbean Sea near the coasts, which can determine the formation of vortexes and filaments, as it has been observed in other regions such as of Western Australia (Batteen et al., 1992).

Since the easterly winds are dominant over the year, to deepen on the connection between the wind stress curl and the number of eddy-observations also a coupled SVD analysis has been performed. As in the SST case, for both variables a linear trend and the mean have been removed at each grid point and the residual has been divided by the standard deviation

The first three combined SVD modes between eddy-observations and wind curl anomalies are displayed in Fig. 4.5; Fig. 4.6; Fig. 4.7. The first one explains 25.8% of the total covariability and shows positive values for the wind curl in a large part of the basin (Fig. 4.5, top right). The remarkable exception is found around the southern coasts where anticyclonic anomalies arise. The periodicity of this pattern, as expected, is of around a year (purple line in Fig. 4.5, middle panel) with positive values for the wind curl during the second half of the year (maximum between September and December) and negative during the first half (through February-April. Temporal amplitudes of eddy-observations and wind curl are highly correlated (Fig. 4.5, bottom) suggesting that there could be a causal connection between wind stress and although complementary analysis are required to verify this point.

The change in the wind curl pattern near the coast may indicate the occurrence of coastal upwelling/downwelling. Pérez-Santos et al. (2010) noted that the annual cycle

of surface wind present different features in the Caribbean Sea with a relative maximum wind stress observed in June caused by the Caribbean low-level jet. The strongest wind stress curl occurs during November presumably due to the collapse of the Atlantic warm pool giving new evidence of the importance of local atmosphere-ocean coupling. Variability at synoptic scale was detected during fall and winter, leaving spring and summer almost free from these activities. The correlation between both series is high (over 80%) with a 12 month periodicity (Fig. 4.5, bottom). A further discussion between wind stress and SST is provided in the following Chapter. A point to note on the temporal amplitudes is the apparently strong inter-annual variability since the range of the amplitudes changes substantially among the years.

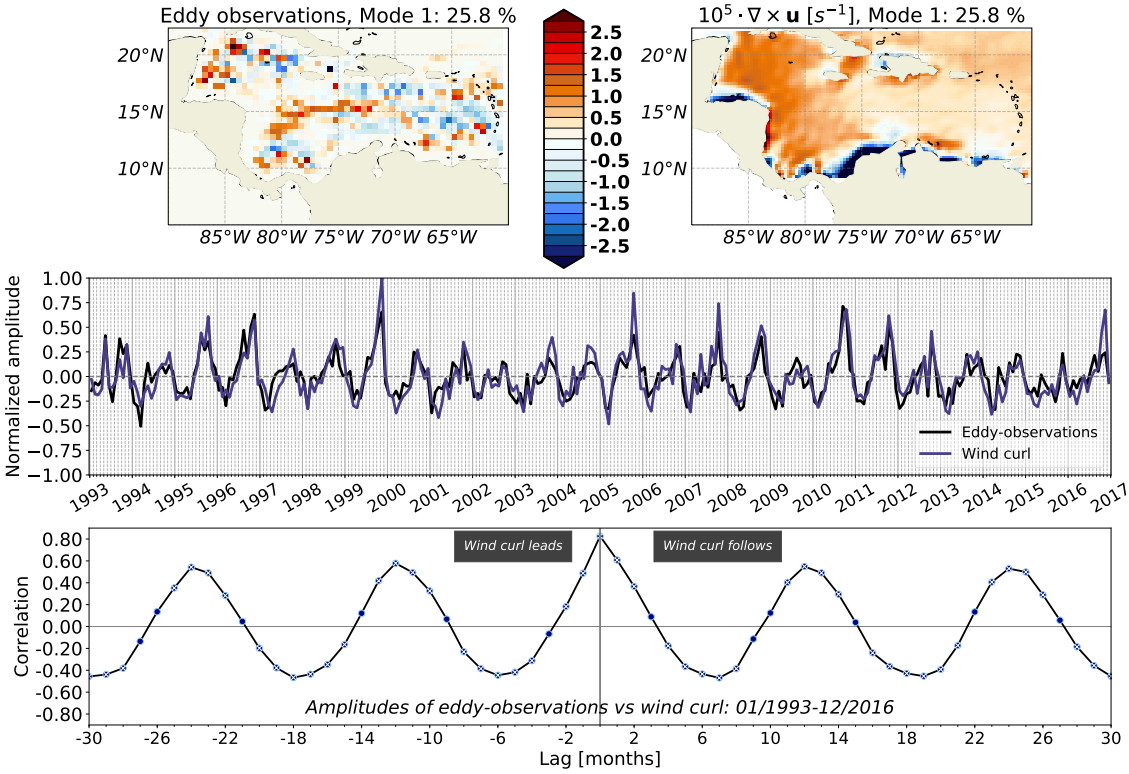

Figure 4.5: Top: First SVD spatial mode for the eddy-observations (left) and for wind curl (right). Center: Corresponding temporal amplitudes for eddy-observations (black) and for the wind curl (purple). Bottom: Cross-correlation between both temporal amplitudes shown in the middle panel.

The second mode, which accounts for 19% of the covariability, is displayed in Fig. 4.6. The spatial pattern for the wind curl (Fig. 4.6, top-right), shows an area around 9° N with intense values of wind curl that is strongest and positive during December and weakest and negative during June (see Fig. 4.6 blue line in the middle panel). This mode is characterized by weak wind curl anomalies in the middle of the Caribbean Sea. As noted by Rodriguez-Vera et al. (2019), although the general wind pattern is westerly all around the year, there is a large seasonal variability. Easterly positive anomalies in the southern side of the domain are present from March to October-November when it weakens, changing

its direction southwards. This result is in accordance with the displacement of the ITCZ at the end of the year. The temporal amplitudes associated with the second mode (Fig. 4.6, middle panel) are correlated up to 80% presenting a periodicity of 12 months. However, the spatial distribution of eddies from this mode is opposed to the first one when the sign of the amplitude is positive. Thus, those areas where in the first mode showed above the average eddy-observations, now denote a reduced presence of eddies.

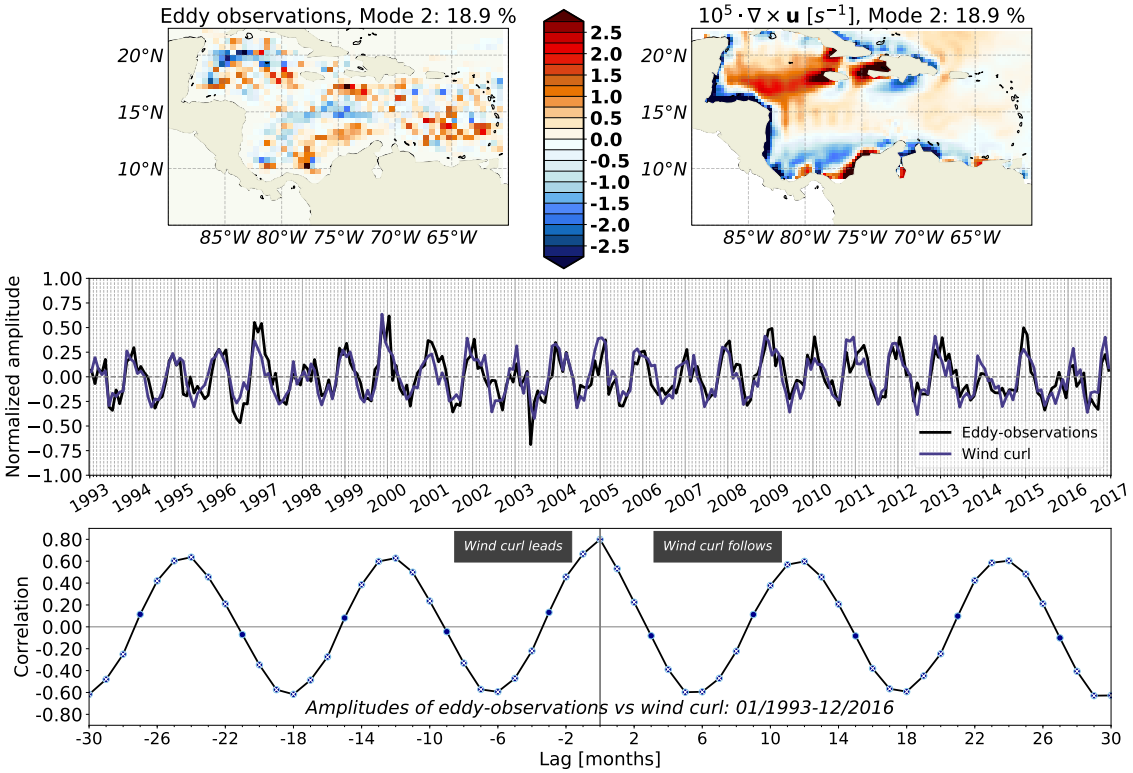

Figure 4.6: Top: second SVD spatial mode for eddy-observations (left) and wind curl (right) anomalies. Center: corresponding temporal amplitudes associated to first row modes for eddy observations (black) and for the wind curl (purple). Bottom: ross-correlation between both temporal amplitudes shown in the middle panel.

Finally, the third SVD mode, wich accounts for 11% of the total variability, shows a similar pattern in the wind curl to the one shown in the second mode (Fig. 4.7). This is a typical situation in the SVD analysis of a process with two periodicities. The amplitudes of both signals are correlated up to a 80% but the periodicity in the correlation is around 6 months, representing in this case a semi-annual oscillation.

4.1.3 Seasonal pattern through SOM decomposition

Once the coupled SVD analysis has revealed the existence of a remarkable seasonal cycle in the number of eddy-observations for some specific Caribbean Sea areas, now a further assessment of the spatial variability of eddy-observations at seasonal scale is

performed through the computation of the Kohonen Self-Organizing Map (SOM), which was described in Section 2.

Thus, the spatial SOM-analysis is applied to the monthly anomalies of eddy-observations. The 4×4 SOM array results are shown in Fig. 4.8 and the percentage of occurrence of each pattern in Fig. 4.9.

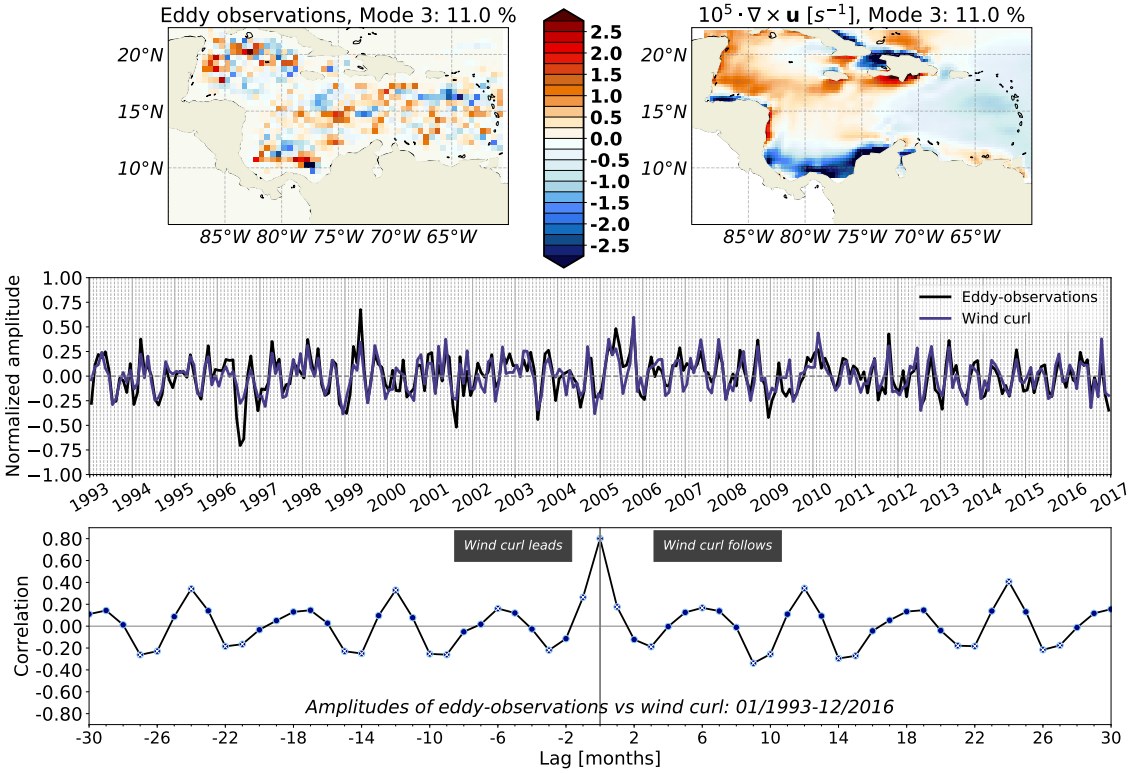

Figure 4.7: Top: third SVD spatial mode for eddy-observations (left) and for wind curl (right). Center: corresponding temporal amplitudes for eddy-observations (black) and for wind curl (purple). Bottom: cross-correlation between both temporal amplitudes shown in the middle panel.

The lowest percentage is explained by P15 (3.12%) and the highest by P1(8.7%). However, P13 and P14 (both with 8.33%) are strikingly similar with little differences only noticeable at the coastal seas. Note that SOM splits the patterns to have topological continuity between the neurons, and thus some of the spatial pattern are necessary for the transition to the next neuron.

The top row of the array is populated by two spatially coherent areas with values above the mean number of eddy-observations. These patches follow the Panama-Colombian gyre near the coast and the Caribbean current along the Yucatan channel respectively. Patterns located in the bottom row, display a unique area with above the mean eddy-observations in the central part of the domain.

Similar patterns are located adjacent to one another in this SOM mapping, while dis-

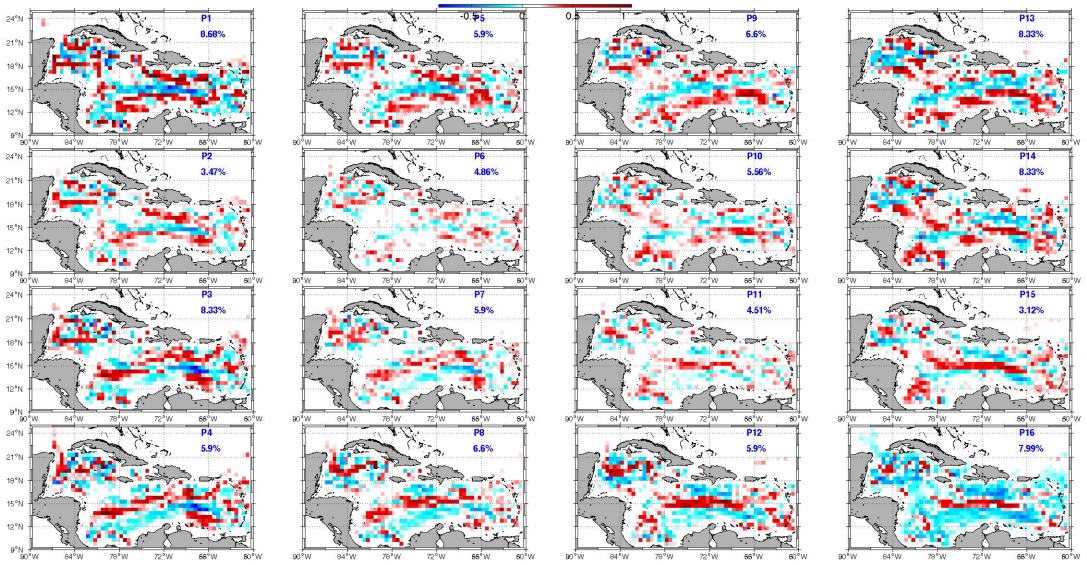

Figure 4.8: Patterns provided by the 4×4 neurons. The number inside each map corresponds to the explained variance.

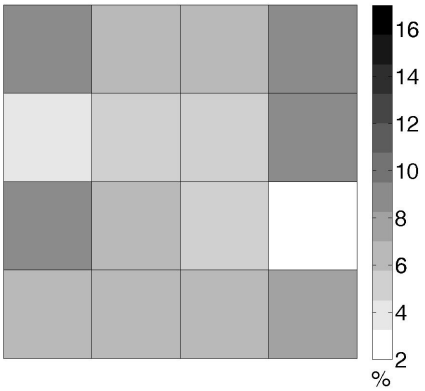

Figure 4.9: Percentage of occurrence by each pattern shown in Fig. 4.8.

similar patterns are at opposite ends of the SOM space, with a continuum of change occurring across the neural network. For each time frame (spatial snapshot) of the time series, the best matching unit (BMU), or the "winner neuron" can be identified according to the minimum Euclidean distance when that frame od the input data is compared to the 16 SOM units. The temporal evolution and the frequency of occurrences of these patterns are shown in Fig. 4.8 where, as expected, it reflects a seasonal modulation of the identified patterns. The BMU (best matching unit) for the monthly data shows a seasonal distribution of patterns in agreement with the SVD (Figure 4.10).

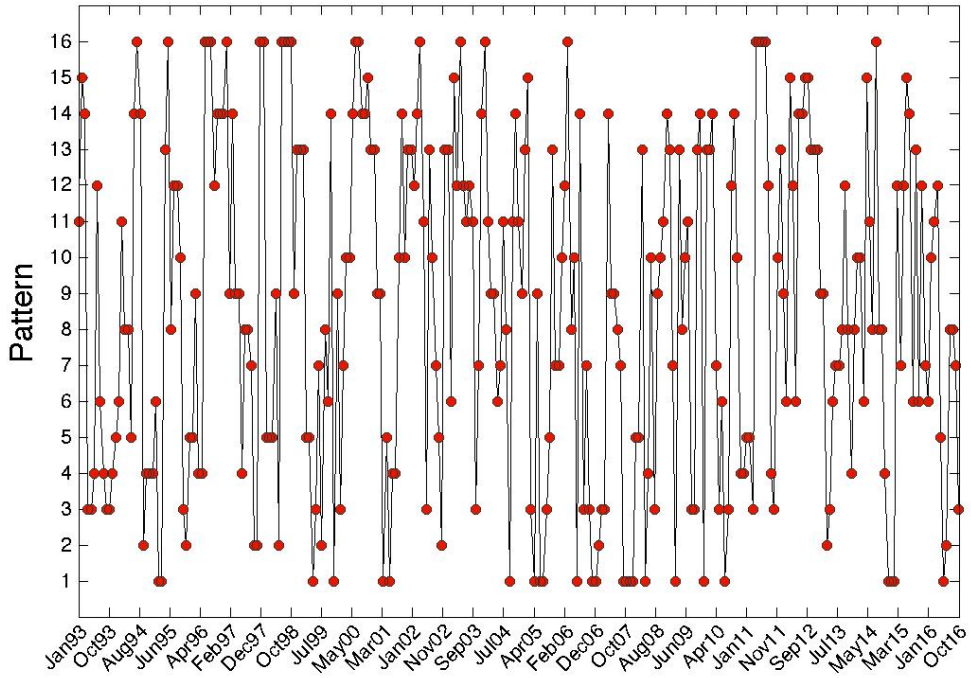

Figure 4.10: Time series of the best matching units.

To gain a better insight of the seasonality of this distribution, we compute the percentage from the BMUs grouped by the four seasons: "Dry" (December-March), "Transition" (April-May), "Veranillo" (Jun-Aug) and "Wet" (Sep-Nov). The probability of occurrence for the four seasons are shown in Fig. 4.11, which reflects more clearly that each season is characterized by a reduced subset of patterns. The "Dry" season, is mostly represented by P13 with an explained variance of 20%. Indeed during that season the distribution of eddy anomalies are mostly represented (around 60%) by the first row of the neuronal pattern which is the situation previously explained. The "Transition" season is mostly explained by P6 which characterizes a basin poorly populated by eddies. The "Veranillo" season is represented by P16 showing above the mean eddies in the central

part of the basin. Finally, the “Wet” season has the most changing spatial pattern of eddy-observations (none of them having null representation) although the most probable are P3 and P14 (with 12 and 17% of probability respectively). P3 displays an eddy transition from the central basin towards Panama and P14 a concentration of eddy-observations in the Colombia-Panama basin and a path through the Yucatan channel.

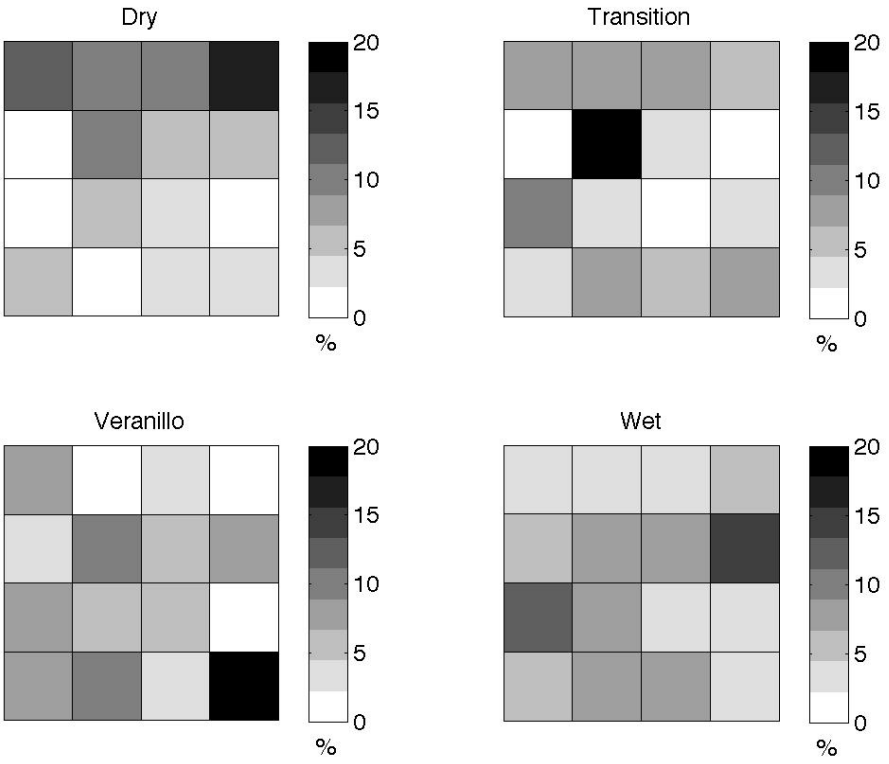

Figure 4.11: Seasonal percentage of explained variance provided by each SOM pattern.

4.2 Inter-annual variability

El Niño Southern Oscillation (ENSO) is an ocean-atmosphere feedback that influences climate variability in several parts of the globe through a phenomena known as teleconnections. Oceanic and atmospheric conditions in the Pacific tend to fluctuate between El Niño (warmer than usual central and eastern Pacific) and La Niña (colder than usual eastern Pacific). Fluctuations are rather irregular, but tend to appear every two to seven years. A more intense phase of each event may last for about a year (such as the strong 1997 and 2015 El Niño events). A warming climate may contribute to a change in the frequency and intensity of the El Niño phenomenon, as it is evidenced by the higher frequency of El Niño Modoki events, with warmer SST anomalies stalled in the central Pacific in turn of the eastern Pacific (Freund et al., 2019). In the northern South America, El Niño leads to a deficit of rainfall along the Caribbean coasts. By contrast, rainfall increases on the coasts of Ecuador, the northern part of Peru, and southern zones of Chile. In Colombia, Venezuela, and Guyana the precipitation tends to decrease, even leading to drought in the northeast of Brazil. Despite the importance of this phenomena in the region, little is known about the influence of ENSO in the variability of currents and hydrography in the southern Caribbean Sea.

ENSO events can be identified by several oceanic Niño indexes, all of which are based on SST anomalies averaged across a given region. Usually the anomalies are computed relative to a base period of 30 years. The numbers of Niño 1,2,3, and 4 correspond with the labels assigned to ship tracks that crossed these regions. The region covered by the Niño 1+2 index ($0 - 10°$S, $90°$W-$80°$W) is the smallest and eastern-most region of all El Niño indexes, and corresponds with the area of coastal South America where El Niño was first recognized by the local population [2]. This index tends to have the largest variance of all Niño SST-based indexes. The Niño 3 region ($5°$N-$5°$S, $150°$W-$90°$W) was once the primary focus for monitoring and predicting El Niño, but researchers later learned that the key region for coupled ocean-atmosphere interactions associated with the ENSO lies further west (Trenberth, 1997). Hence, the Niño 3+4 (which lies between El Niño 3 and El Niño 4, also called the Oceanic Niño Index, ONI) became favored to identify El Niño and La Niña events. The Niño 3+4 ($5°$N-$5°$S, $170°$W-$120°$W) anomalies may be thought as a representation of the average equatorial SST across the Pacific from about the dateline to the coast of South America.

The lagged correlation between the monthly time series of anomalies of eddy observations and the different El Niño indices is shown in Fig. 4.12. All indices show a similar lagged correlation despite some small differences (more noticeable with El Niño 1+2 which is defined in the closest region to Colombia but covers a relatively small area).

[2] This phenomenon was already known in Peru in the sixteenth century. The Paita fishermen called the "Niño Current" the annual income of warm water on Christmas Eve, which coincided with "the arrival of the Niño Dios".

A significant correlation at 95% exists around lag $\tau = -24$ months, which indicates that a positive ENSO may be associated an increment of eddies in the Caribbean basin. Indeed the periodicity of the ENSO phenomenon is marked in the correlation since it is not symmetrical and two consecutive events are separated on average about 40 months (significant correlation at lag $\tau = 16$ months. It is within the range of periodicities known of ENSO episodes (between 2 and 7 years). Because here only it is analyzed the available SSH data the only that can be said is that during this 24 year period, positive ENSO events may be connected with a number of eddies above the mean in the basin while negative ENSO events would reflect the opposite.

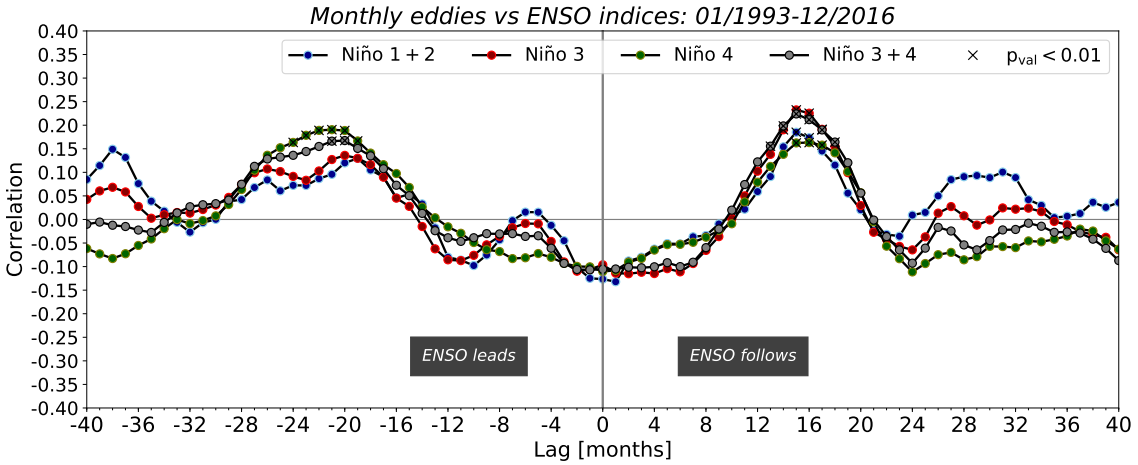

Figure 4.12: Time lag correlation between the monthly eddy time series and Niño 1+2(blue), Niño 3 (red), Niño 4 (green) and Niño 3+4 (brown) .

To further analyze this relation, a cross-wavelet analysis is performed between the monthly time series of eddies and the closest Niño index to the Caribbean Sea (El Niño 1+2). As outlined in Chapter 2, the wavelet transform is a mathematical technique that decomposes a time series into time/frequency space simultaneously. Fig. 4.13 shows the wavelet coherence analysis between both time series (see colorbar), the phase between the correlation (arrows) and the significance of the correlations at 95% (black contours). Note the cross-hatched U-shaped curve at the bottom of the plot. This area is located in the Cone of Influence (COI), where values are impacted by the frequency being too short (or the period too long) to correctly sample parts of the time series. As the period gets longer, the COI becomes larger. Statistical significance (shading) is shown at a time/frequency point where the normalized power is greater than 1. The time series is lined up with the power plot on the left. The page can return the same plot but not show/use values from within the COI (note that in this case the total variance is not explained by the wavelet).

It can be seen that around 1998 there is a significant anticorrelation between both time series in a characteristics period of around 20 months during which time series are in phase (maximum in one time series coincides with a maximum in the other). Indeed

during 1995-1997 there was a long La Niña event recorded. [3].

A significant correlation is also present for a period of 16 months in 2008, but in this case it is $\pi/2$ out of phase, which corresponds to a difference of the phase of 4 months between ENSO and the number of eddies-observations. Also, an anticorrelation is presented in 2008 at the characteristics period of around 6 months. Other periodicities appear in Fig. 4.13 but they are not statistically significant to be discussed in more detail.

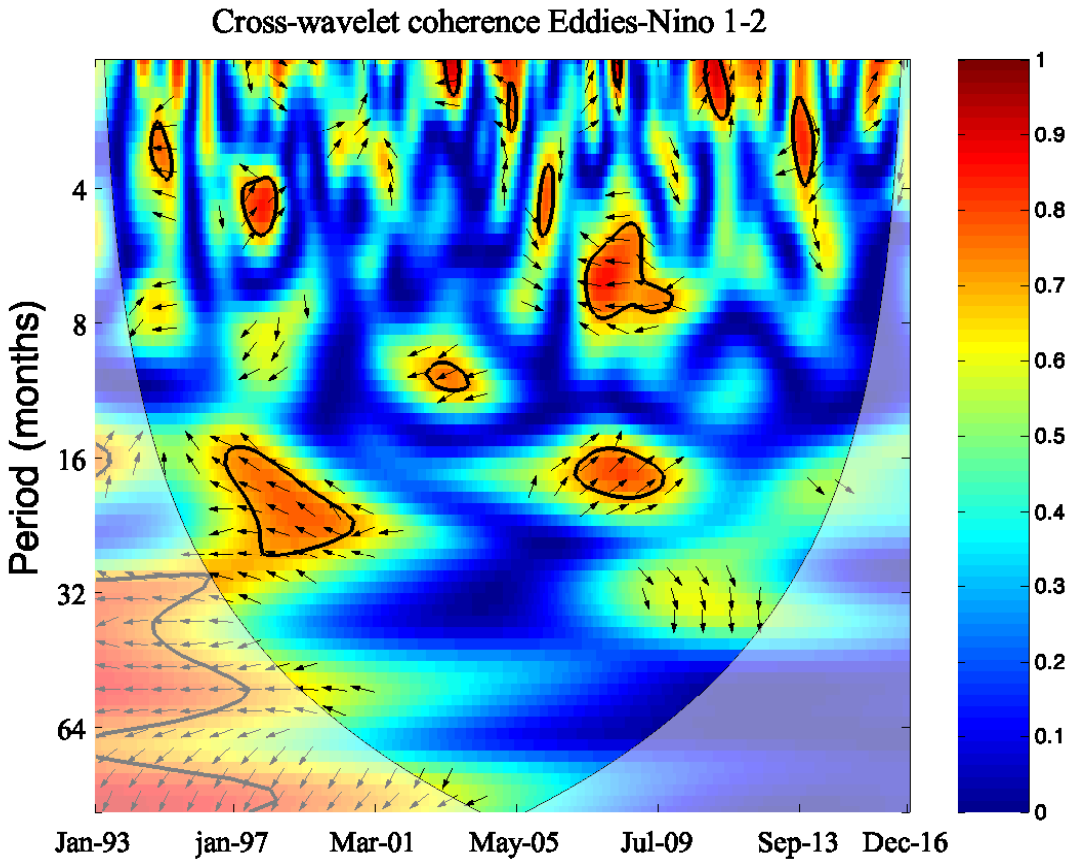

Figure 4.13: Wavelet cross-correlation between monthly eddy-observations and El Niño 1+2 index. Black contours indicate a significant correlation at 95%. Arrows indicate the phase of the cross-correlation as follows: if pointing right the number of eddies in the Caribbean Sea and El Niño 1+2 index are in-phase, if pointing left both are in anti-phase, if pointing down (that is -90º from the horizontal), it means that the two signals are out of phase -1/4 of the period/frequency in which the number of eddies in the Caribbean Sea leads El Niño 1+2 index. In the case that they point upwards it is the same but the lag is 3/4 times the period/frequency at which El Niño 1+2 leads the number of eddies in the Caribbean Sea.

[3] https://climatedataguide.ucar.edu/climate-data/nino-sst-indices-nino-12-3-34-4-oni-and-tni

Chapter 5

Discussion and Conclusions

The work presented in this Thesis describes the main statistical characteristics as well as the seasonal and inter-annual variability of mesoscalar eddies derived from SLA in the Caribbean Sea between 1993 and 2016. A better understanding of the variability of eddies, their spatial distribution, and of their relation with climate signals contribute to gain new knowledge on their mechanisms of formation, intensification and dissipation, which have strong implications on biogeochemical and air-sea exchange processes. Since the Caribbean Sea is a semienclosed basin, a large part of the transport of nutrients and heat both in the vertical and in the horizontal dimensions are to a large extent the result of these structures.

The spatial distribution of mesoscale eddies reported in this work is consistent with findings from previous studies in which most of the eddies are formed in the eastern Caribbean Sea, or alternatively, had already formed in the north east of Brazil. Some of them stay some time off the Colombian and Venezuelan coast, while the reminder tend to redistribute around the Cayman and Yucatan basins (e.g. Carton and Chao, 1999; Andrade and Barton, 2000; Oey and Lee, 2003; Jouanno et al., 2008; Richardson, 2005; Jouanno et al., 2009; Chelton et al., 2011b). The prevalent travelling direction for both cyclonic and anticyclonic polarities is westward feeding the Caribbean boundary current. Among these, 816 are cyclonic and 897 anticyclonic. The number of eddies that propagate eastward is smaller, of which 109 are anticyclonic and 72 are cyclonic. As already pointed out in Chelton et al. (2011b) the most noticeable characteristic of the eastward-propagating eddies is that, they have quite shorter propagation distances than the westwards one. Here, no significant differences between the distances traveled by both polarities (see Fig. 3.6) are found. Moreover, it is suggested that the instability of the main Caribbean current is the most relevant explanation for the growth of the mesoscale eddies in the Caribbean Sea and that NBC rings trigger an instability which would occur anyway as pointed out in Jouanno et al. (2009). These perturbations can generate larger eddies that grow in size and strength as they move westward to the Colombian basin (Jouanno and Sheinbaum, 2012), taking approximately 180 days to cross the basin be-

fore dissipating near the coast of Nicaragua or the Yucatan peninsula (e.g. Carton and Chao, 1999). Although many works (e.g. Carton and Chao, 1999; Oey and Lee, 2003; Richardson, 2005; Jouanno et al., 2008; van der Boog et al., 2019) have presented preferences for anticyclonic polarities in the Caribbean sea, in this work there is no significant difference between cyclonic (46.8 %) and anticyclonic (53.11 %) eddies, neither in their respective origin, propagation, amplitude or radius but in the parameter of non-linearity which shows greater non-linearity for anticyclonic eddies (see Fig. 3.1).

Jouanno et al. (2008) found that the largest eddies in the Caribbean sea are anticyclonic, which travel westward with a radius between 200 and 500 km and have a lifetime between 50 and 110 days. These eddies are thought to be intensified by freshwater river plumes and upwelling events, as they increase the density gradient between the coast and the interior, thus reinforcing the thermal wind balance as they move to the west where the background density and the velocity shear are larger (van der Boog et al., 2019). Our results indicate that the average lifetime for westward propagating mesoscale eddies before dissipation was 68 ± 45 days, and that most of these eddies ($>$ 85%) have a lifetime shorter than 120 days. Comparing the results from Carton and Chao (1999) and Oey and Lee (2003), who found the period of spin-up, growth, and drift is approximately 100 days, and with those from Andrade and Barton (2000), who found that the typical timescale of synoptic eddies travelling through the Caribbean Sea is between 100-130 days, it can be concluded that there is no difference between polarities although there is a general agreement with their longevity.

The mean radius detected, 105.0 ± 30.0 km for cyclonic and 97.5 ± 28.3 km for anticyclonic eddies does not agree with the one provided by Jouanno et al. (2008), although our results are consistent with the latitudinal distribution of eddy sizes described by Chelton et al. (2011b), in which eddies of around 200 km of radii are found in the near-equatorial regions to monotonically decrease up to 80 km at 20° of latitude. We note that these length–scales of eddies and eddy–like features are constrained by the Rossby radius of deformation. On the other hand, the mean value of the amplitude is 6.8 ± 3.6 cm for cyclonic (Fig. 3.3e) and 7.9 ± 4.2 cm for anticyclonic eddies (Fig.3.3f). This result is consistent with the work from Gaube (2013), who found that the eddy field in the Caribbean Sea is characterized by mesoscale eddies with average amplitudes of 7.8 cm, as well as with the latitudinal variation of the zonally averaged eddy amplitude found in Chelton et al. (2011b). However, as noted in Chelton et al. (2011b), the predominance of small eddy amplitudes can be influenced by the procedure applied in the detection of eddies which may sometimes be biased by 1 or 2 cm in regions with very energetic mesoscale variability and by less than 1 cm in less energetic regions due to the complex geometry of many eddies. Since we have not found any remarkable difference between both polarities in the above mentioned properties, we proceeded to normalize the amplitude, radii and non-linearity of eddies according to their lifetime, where the anticyclonic eddies increase

slightly in amplitude and reaching the maximum radii faster than cyclones ones (see Fig. 3.3). From here, the normalized eddy properties according to their lifetime suggest that, the lifetime of an eddy may be predicted once the peak of the amplitude has been reached, which suggest to slightly change the statement of Chelton et al. (2011b) from “the amplitude of an eddy is not enough to determine its longevity" to “the amplitude of an eddy may be enough to determine its longevity if regional lifetime patterns are known".

Eddies mostly dissipate near the coast of Nicaragua or the Yucatan peninsula and only few of them are able to travel northwards crossing the Yucatan basin as already noted by Carton and Chao (1999) and Chelton et al. (2011b), who pointed out that eddy disappearance is more frequent near the western boundaries. However, eddy dissipation in the open ocean can occur by frictional decay or coalescence with other eddies as a consequence of the up-scale energy cascade of geostrophic turbulence. Some of these terminations may also occur from temporary or permanent loss of an eddy by the tracking procedure because of noise in the SSH field or imperfections of the tracking algorithm (Chelton et al., 2011b). In this regard, Amores et al. (2018) also noted that the number of detected eddies can be significantly underestimated due to the interpolation and filtering methods behind the construction of gridded SLA fields, which can be removing some real SLA eddy-like anomalies. Besides, the transfer of vorticity from the atmosphere to the ocean and the seasonal variability in the atmospheric forcing may play an important role in the dissipation of eddies in the basin.

Only few eddies are able to pass through the Chibcha Channel to the Cayman Sea. Eddies which originated in the southwestern Caribbean Basin are the only ones not advected by the Caribbean current nor affected by its instabilities. These eddies tend to remain in the southwestern Caribbean Sea where they form distinctive SLA patterns. Richardson (2005) pointed out that many anticyclonic eddies travel westwards up to the Jamaica Ridge when they are disrupted by topographic-induced dissipation.
The density of eddy dissipation in the Central American Rise, near the coast of Nicaragua, the Yucatan peninsula, in the Panama–Colombia Gyre and in the open basin can be seen in Fig. 3.8) agreeing well with the data provided by Rodríguez-Rubio et al. (2003).

The seasonal variability and the spatial distribution of eddies differ with the eddy polarity although the seasonal distribution in the spatial density of eddies is almost similar. The position of the ITCZ over the southwestern Caribbean during part of the year induces a maximum precipitation and wind patterns (eastern upwelling events) that favour a significant increase of freshwaters thus creating meridional and zonal salinity gradients. Monitoring the wind stress can help to detect these kind of events, which are also partly reflected in the wind curl as was seen in the previous section and was already suggested in Andrade and Barton (2000) since the formation of eddies was linked with the interaction between the meandering Caribbean boundary Current and the wind curl, as has

been explored in the previous section. Also Jouanno and Sheinbaum (2012) showed that the variations of the eddy activity in the Caribbean Sea respond to changes in the mean flow and found two EKE maxima occurring during March–April and September–October, as the result of the local enhancement of the conversion from barotropic to baroclinic energy during these periods by an increase of instabilities. The seasonal variability of the EKE in the Colombia Basin is not clearly connected with the variability further east, in the Venezuela basin, which is clearly dominated by an annual cycle. Based on the assessment of the number of eddies in square cells presented in Section 4, it has been found that the number of eddies is larger during the Dry season with 36 % of the total westwards propagating eddies. During the Transition season, approx. 18 % of the total eddies with westward propagation have an important distribution in the whole Colombia Basin, while during the Veranillo de San Juan season, 23% of the eddies propagate westward. Most of theses eddies develop at the eastern side of the basin. Finally, during the wet season, 22% of the analyzed eddies traveled westward, the majority of them formed in the Colombian basin. On the other hand, the eastwards propagating eddies show significant differences in both eddy polarities during the Dry and Veranillo de San Juan seasons. The dry season is characterized by less cyclonic than anticyclonic eddies in the Yucatan Basin, while the opposite occurs in the northwestern Colombian basin. Main differences in Veranillo de San Juan season are concentrated in the Colombian and in the southern part of Venezuela Basins where more anticyclonic eddies are detected.

Spectral analysis for the daily and monthly eddy-observations over the region does not show any clear periodicity although some spectral energy peaks appear at the semi annual and annual periods not being totally conclusive. As pointed in Alvera-Azcarate and Barth (2009), SSH varies at the annual scale mainly by a seasonal steric effect and at longer cycles the SSH slope across the intensity of the Caribbean Current. These authors suggested already a seasonality in the formation of eddies since half of the observed eddies detached from the Loop Current from July to September. A relation is also found between the intrusion of the Loop Current into the Gulf of Mexico and the size of the eddies shed from it; larger intrusions trigger smaller eddies. While the annual cycle consists mainly of a steric variation as reflected in the response of the surface layers to the heat fluxes, it has been suggested that interannual variations (occurring over an approximate 4–yr cycle), consist of variations of the north–south slope across the Caribbean Current that affect the geostrophic transport. Our results indicate that this cycle could affect the eddy density at both polarities cyclonic and anticyclonic since some energy at 0.02 cycles/months (around 4 years) is visible in the spectra (Fig. 4.2).

Density of eddy observations is annually anti-correlated with SST (correlation of 0.8) following a pattern defined by the spatial map of the complex SVD. When the SST is above the mean, the Colombian and Venezuela basins present less eddy activity while near the Yucatan Channel and in the mid-western Caribbean Sea occurs the opposite

presenting more eddies during the summer season. As already mentioned, anticyclonic eddies are thought to have formed in the eastern Caribbean from the anticyclonic vorticity derived from North Brazil Current rings (Richardson, 2005). The ring vorticity enters the eastern Caribbean through island passages and is probably amplified by the anticyclonic shear on the northern side of the jets.

Based on the SVD coupled analysis between monthly anomalies of eddy-observations and wind-curl it is found that the first mode explains 25.8% of the total covariability and has annual cycle. Wind curl anomalies have a positive value in the interior during late summer/fall and in the boundary during winter/early spring (Fig. 4.5 top and middle panels). Temporal amplitudes of eddy-observations and wind curl appear to be highly correlated thus revealing the annual cycle of eddy density anomalies (Fig. 4.5 bottom panel). Andrade and Barton (2000) showed that both high SLA and EKE values are observed in the center of the basin during July-October, which suggested them that the enhancement in the number of eddies is directly related with the maximum curl of the north trade winds at the core of the low-level jet. As said above, the position of the ITCZ over the southwestern Caribbean during part of the year produces an intense precipitation maximum and curl maximum in the wind field. Likely the eddies formed there are driven by the consequent meridional and zonal salinity gradient and by the direct action of both wind curl and stress. Besides, a change in the wind curl near the coast possibly indicates the occurrence of coastal upwelling/downwelling, a subject that has been largely studied in the Guajira.

The second coupled SVD mode accounted for 19% of the covariability and showed intense values of wind curl at around 9°N, which strengthen (positive) during December and weaken (negative) during June. Those weak wind curl anomalies in the middle of the Caribbean Sea may reflect the displacement of the ITCZ at the end of the year (Fig. 4.6 top panels). The temporal amplitudes associated to eddy density and wind curl anomalies of this second mode are also correlated up to 80% with a periodicity of 12 months. However, the spatial distribution of eddies from this mode is opposite to the first one suggesting a double effect of the general wind pattern and that the fluctuation of the ITCZ affects the presence of eddies in the basin. As pointed out in Jouanno and Sheinbaum (2012) Caribbean eddies are not generated directly by the local wind and the importance of the wind field for the Caribbean mesoscale variability is indirect. This is in accordance with the results obtained in this Thesis where two different behaviours are observed for the first two coupled SVD modes between eddies and wind, the first one accounting for the seasonal wind variability over the area and the second describing the meridional displacement of the ITCZ at annual scale. However, it is also possible that local wind stress curl can form anticyclones. It was demonstrated in Oey and Lee (2003), who using a numerical simulation of Caribbean ocean circulation found that a patch of anticyclonic wind stress curl located southwest of Hispaniola can force a depression of isopycnals through Ekman pumping, resulting in an anticyclone. These “Hispaniola anticyclones”, as they

called them, subsequently drifted westward through the Caribbean Sea at a rate of about 3–4 per year.

Moreover, a seasonal classification of the spatial distribution of eddy-observations through a neural network based on Self Organized Maps (SOM) shows that the most representative patterns differ when the analysis is performed by seasons. The only common pattern that coexist between seasons is P8 that appears in the Dry and Transition seasons and P5 in Veranillo and Wet seasons but with different explained variance (Fig. 4.8). The most representative patterns for the different seasons are P8, P12, P15 and P16 for the Dry season, P3,P4,P7 and P8 for the Transition season, P1,P2 and P5 for the Veranillo season and P5, P9, P13 and P14 for the wet season. This complex spatial distribution of eddies has a periodicity that needs to be further analyzed in future research (Fig. 4.10)

At inter-annual scale, the density of eddy-observations has a correlation with the oceanic ENSO indexes of about 0.2 with a lag of $\tau = -24$ months (Fig. 4.12). Despite the correlation is relatively low, this result suggests that a positive ENSO is reflected in an increment in the number of eddies in the Caribbean basin. Zamudio et al. (2001) pointed out that strong ENSO events are characterized by warm phase or downwelling Kelvin waves that destabilize the upper ocean circulation with three consecutive effects: first, a coastal jet characterized by strong vertical shear flow develops; then the shear flow strengthens, increasing its horizontal dimension and the amplitude of its oscillations and, finally, the jet becomes unstable and breaks into anticyclonic eddies, which separate from the coast and drift southwestward. The genesis and strengthening of the jet responds to the simultaneous occurrence of the poleward-flowing currents along the southwest coast of Mexico and the poleward circulation associated with ENSO downwelling Kelvin waves. Inter-annual fluctuations of ENSO indexes are rather irregular, but tend to appear every three to six years. A more intense phase of an episode may last for about a year. A warming climate may contribute to an increase in the frequency and intensity of ENSO events (Cai et al., 2018). Regarding its impact on the Caribbean basin, it is well known that a positive ENSO phase leads to a deficit of rainfall in northern South America. Therefore if rainfall decreases river runoff into the Caribbean Sea, which helps to form salinity gradients (van der Boog et al., 2019), can also be negatively impacted. These changes may be reflected in a weakening (lower amplitude) of those eddies that move westward along the boundary current, thus decreasing their lifetime and traveled distance. To better know how the global warming induces changes in rainfall, wind patterns and ocean currents may affect the formation of eddies it is necessary the implementation or assessment of dedicated numerical simulations, which is far beyond from the scope of this Thesis.

However, from a wavelet analysis it was found that around 1998 there is a significant anticorrelation between both time series in a characteristics period of around 20 months during which time series are in phase (maximum in one time series coincides with a max-

imum in the other). Indeed during 1995-1997 there was a long La Niña event recorded (Fig. 4.13). Significant correlations also exist for 2009 but, in that case it is $\pi/2$ out of phase, which corresponds to the negative phase of the ENSO index thus coinciding with a moderate La Niña episode recorded between 2007 and 2009.

Recommended future research to extend the present Thesis includes the spatio-temporal characterization of other eddy-characteristics such as SST, heat fluxes and primary productivity using state-of-the-art satellite data, as well as the comparison of shown observational results with those provided by model simulations. Eddies can easily be tracked in model outputs and their properties evaluated with more detail since all the information about the current fields and on the water masses that they transport is available for the whole column of water (3D). To conclude, regarding climate scales, a more accurate characterization of changes in eddy properties such as their lifetime or their amplitude with climate signals such as the ENSO, the NAO or the PDO can be performed with the more recent eddy Atlas dataset that includes information from eddies until the end of 2019.

Bibliography

Alvera-Azcarate, A. and Barth, A. (2009). The surface circulation of the caribbean sea and the gulf of mexico as inferred from satellite altimetry. *Journal of Physical Oceanography*, 39.

Amores, A., Jordà, G., Arsouze, T., and Sommer, J. L. (2018). Up to what extent can we characterize ocean eddies using present day gridded altimetric products. *American Geophysical Union*.

Andrade, C. A. (1993). Analysis of the surface-wind speed over the caribbean sea. *Bull. Sci. Cent. Invest. Oceanogr. Hidrogr.*, 13:33–44.

Andrade, C. A. (2000). *The circulation and variability of the Colombian Basin in the Caribbean Sea*. PhD thesis, University of Wales.

Andrade, C. A. and Barton, E. D. (2000). Eddy development and motion in the caribbean sea. *Journal of Geophysics Research*, 105(C11):26191–26201.

Andrade, C. A. and Barton, E. D. (2005). The guajira upwelling system. *Continental Shelf Research*, 25(9):1003 – 1022.

AVISO (2017). *Mesoscale Eddy Trajectory Atlas Product Handbook*.

Batteen, M. L., Rutherford, M. J., and Bayler, E. J. (1992). A numerical study of wind- and thermal-forcing effects on the ocean circulation off western australia. *Journal of Physical Oceanography*, 22(12):1406–1433.

Baums, I. B., Paris, C. B., and Chérubin, L. M. (2006). A bio-oceanographic filter to larval dispersal in a reef-building coral. *Limnology and Oceanography*, 51(5):1969–1981.

Beier, E., Bernal, G., Ruiz-Ochoa, M., and Barton, E. D. (2017). Freshwater exchanges and surface salinity in the colombian basin, caribbean sea. *PLoS ONE*.

Beron-Vera, F., Olascoaga, M. J., Haller, G., Farazmand, M., Triñanes, J., and Wang, Y. (2015). Dissipative inertial transport patterns near coherent Lagrangian eddies in the ocean. *Chaos: An Interdisciplinary Journal of Nonlinear Science*, 25(8):087412.

Brannigan, L., Marshall, D. P., Garabato, A. C. N., and Nurser, A. G. (2015). Submesoscale instabilities in mesoscale eddies. *Ocean Modelling*, 92:69–.

Brannigan, L., Marshall, D. P., Garabato, A. C. N., Nurser, A. G., and Kaiser, J. (2017). Submesoscale instabilities in mesoscale eddies. *Journal of Physical Oceanography*.

Cai, W., Wang, G., Dewitte, B., Wu, L., Santoso, A., Takahashi, K., Yang, Y., Carréric, A., and McPhaden, M. J. (2018). Increased variability of eastern pacific el niño under greenhouse warming. *Nature*, 564(7735):201–206.

Carton, J. A. and Chao, Y. (1999). Caribbean sea eddies inferred from topex/poseidon altimetry and a $1/6^{\circ}$ atlantic ocean model simulation. *Journal of Geophysical Research*, 104.

Castelao, R. M. and Barth, J. A. (2006). Upwelling around cabo frio, brazil: The importance of windstress curl. *Geophysical Research Letters*, 33.

Castelao, R. M. and Barth, J. A. (2007). The role of wind stress curl in jet separation at a cape. *Journal of Physical Oceanography*, 37.

Centurioni, L. R. and Niiler, P. P. (2003). On the surface currents of the caribbean sea. *Geophysical Research Letters*, 30.

Chaigneau, A., Gizolme, A., and Grados, C. (2008). Mesoscale eddies off peru in altimeter records: Identification algorithms and eddy spatio-temporal patterns. *Progress in Oceanography*, 79(2):106–119.

Chelton, D. and Schlax, M. (1996). Global observation of oceanic rossby waves. *Science*, 272:234–238.

Chelton, D., Schlax, M., Samelson, R., and Szocke, R. (2007). Global observations of large oceanic eddies. *Geophysical Research Letters*, 34.

Chelton, D. B., Gaube, P., Schlax, M. G., Early, J. J., and Samelson, R. M. (2011a). The influence of nonlinear mesoscale eddies on near-surface oceanic chlorophyll. *Science*, 334:328.

Chelton, D. B. and Schlax, M. G. (2003). The Accuracies of Smoothed Sea Surface Height Fields Constructed from Tandem Satellite Altimeter Datasets. *Journal of Atmospheric and Oceanic Technology*, 20.

Chelton, D. B., Schlax, M. G., and Samelson, R. M. (2011b). Global observations of nonlinear mesoscale eddies. *Progress in Oceanography*, 91(2):167 – 216.

Chérubin, L. M. and Richardson, P. (2007). Caribbean current variability and the influence of the amazon and orinoco freshwater plumes. *Deep Sea Research Part I: Oceanographic Research Papers*, 54:1451–1473.

Cipollini, P. and Snaith, H. (2013). A short course on altimetry. In *Altimetry Principles and instruments*. National Oceanography Centre.

Conti, D., Orfila, A., Mason, E., Sayol, J. M., Simarro, G., and Balle, S. (2016). An eddy tracking algorithm based on dynamical systems theory. *Ocean Dynamics*, 66(11):1415–1427.

Cullen, V. (Cullen, V., 2005:). Down to the sea for science: 75 years of ocean research, education, and exploration at the woods hole oceanographic institution. *Woods Hole Oceanographic Institution*.

Faghmous, J. H., Frenger, I., Yao, Y., Warmka, R., Lindell, A., and Kumar, V. (2015). A daily global mesoscale ocean eddy dataset from satellite altimetry. *Scientific Data*, 2:150028 EP –. Data Descriptor.

Farmer, D., Pawlowicz, R., and Jiang, R. (2002). Tilting separation flows: a mechanism for intense vertical mixing in the coastal ocean. *Dynamics of Atmospheres and Oceans*, 36(1):43 – 58. Ocean Fronts.

Freund, M. B., Henley, B. J., Karoly, D. J., McGregor, H. V., Abram, N. J., and Dommenget, D. (2019). Higher frequency of Central Pacific El Niño events in recent decades relative to past centuries. *Nature Geoscience*, 12(6):450–455.

Gaube, P. (2013). *Satellite Observations of the Influence of Mesoscale Ocean Eddies on Near-Surface Temperature, Phytoplankton and Surface Stress*. PhD thesis, Oregon State University.

Gaube, P., Chelton, D., Samelson, R. M., Schlax, M. G., and O'Neill, L. W. (2015). Satellite observations of mesoscale eddy-induced ekman pumping. *Journal of Physical Oceanography*, 45.

Gaube, P., Chelton, D. B., Strutton, P. G., and Behrenfeld, M. J. (2013). Satellite observations of chlorophyll, phytoplankton biomass, and ekman pumping in nonlinear mesoscale eddies. *Journal of Geophysics Research: Oceans*, 118:6349–6370.

Goni, G. J. and Johns, W. E. (2003). Synoptic study of warm rings in the north brazil current retroflection region using satellite altimetry. In Goni, G. and Malanotte-Rizzoli, P., editors, *Interhemispheric Water Exchange in the Atlantic Ocean*, volume 68 of *Elsevier Oceanography Series*, pages 335 – 356. Elsevier.

Haller, G. (2015). Lagrangian coherent structures. *Annual Review of Fluid Mechanics*, 47(1):137–162.

Hellweger, F. L. and Gordon, A. L. (2002). Tracing amazon river water into the caribbean sea. *Journal of Marine Research*, 60(4):537–549.

Henson, S. A. and Thomas, A. C. (2008). A census of oceanic anticyclonic eddies in the gulf of alaska. *Deep Sea Research Part I: Oceanographic Research Papers*, 55(2):163 – 176.

Herbaut, C., Mortier, L., and Crepon, M. (1996). A sensitive study of the general circulation of the wetern mediterranean sea. part i: The response to density forcing through the straits. *American Meteorological Society*.

Hughes, C. W., Williams, J., Hibbert, A., Boening, C., and Oram, J. (2016). A rossby whistle: A resonant basin mode observed in the caribbean sea. *Geophysical Research Letters*, 43:7036–7043.

Iselin, C. and Fuglister, F. (1948). Some recent developments in the study of the gulf stream. *J. Mar. Res*, 7:317–329.

Jaimes, B. and Shay, L. K. (2015). Enhanced wind-driven downwelling flow in warm oceanic eddy features during the intensification of tropical cyclone isaac (2012): Observations and theory. *Journal of Physical Oceanography*, 45:1667–1689.

Jochumsen, K., Rhein, M., and Böning, S. H. C. W. (2010). On the propagation and decay of north brazil current rings. *Journal of Geophysical Research*, 115.

Johns, W. E., Townsend, T. L., Fratantoni, D. M., and Wilson, W. D. (2002). On the atlantic inflow to the caribbean sea. *Deep Sea Research I*, 49:211–243.

Jouanno, J. and Sheinbaum, J. (2012). Seasonal and Interannual Modulation of the Eddy Kinetic Energy in the Caribbean Sea. *American Meteorological Society*.

Jouanno, J., Sheinbaum, J., Barnier, B., Molines, J.-M., Debreu, L., and Lemarié, F. (2008). The mesoscale variability in the caribbean sea. part i: Simulations and characteristics with an embedded model. *Ocean Modelling*.

Jouanno, J., Sheinbaum, J., Barnier, B., Molines, J.-M., Debreu, L., and Lemarié, F. (2009). The mesoscale variability in the caribbean sea. part ii: Energy sources. *Ocean Modelling*.

Jury, M. R. (2011). Long-term variability and trends in the caribbean sea. *International Journal of Oceanography*.

Kanzow, T., Cunningham, S. A., Johns, W. E., Hirschi, J. J.-M., Marotzke, J., Baringer, M. O., Meinen, C. S., Chidichimo, M. P., Atkinson, C., Beal, L. M., Bryden, H. L., and Collins, J. (2010). Seasonal variability of the atlantic meridional overturning circulation at 26.5 °n. *Journal of Climate*, 23(21):5678–5698.

Liu, L., Silver, D., Bemis, K., Kang, D., and Curchitser, E. (2017). Illustrative Visualization of Mesoscale Ocean Eddies. *Computer Graphics Forum*, 36.

Liu, Y., Weisberg, R. H., Vignudelli, S., and Mitchum, G. T. (2016). Patterns of the loop current system and regions of sea surface height variability in the eastern Gulf of Mexico revealed by the self-organizing maps. *Journal of Geophysical Research: Oceans*, 121(4):2347–2366.

Malanotte-Rizzoli, P. and Bergamasco, A. (1989)). The circulation of the eastern mediterranean sea. part i. *Oceanologica Acta*, 12.

Malanotte-Rizzoli, P. and Bergamasco, A. (1991)). The wind and thermally driven circulation of the eastern mediterranean sea. part ii: the baroclinic case. *Dynamics of Atmospheres and Oceans*, 15.

Mason, E., Pascual, A., and McWilliams, J. C. (2014). A New Sea Surface Height–Based Code for Oceanic Mesoscale Eddy Tracking. *Journal of Atmospheric and Oceanic Technology*, 31(5):1181–1188.

Massel, S. R. (2001). Wavelet analysis for processing of ocean surface wave records. *Ocean Engineering*, 28(8):957 – 987.

McCabe, R. M., MacCready, P., and Pawlak, G. (2006). Form drag due to flow separation at a headland. *Journal of Physical Oceanography*, 36(11):2136–2152.

Molcard, A., Pinardi, N., Iskandarani, M., and Haidvogel, D. (2002). Wind driven general circulation of the mediterranean sea simulated with a spectral element ocean model. *Dynamics of Atmospheres and Oceans*, 35:97–130.

Molinari, R., Spillane, M., Brooks, I., Atwood, D., and Duckett, C. (1981). Surface current in the caribbean sea as deduced from lagrangian observations. *Journal of Geophysical Research*, 86.

Monro, D. M. and Branch, J. L. (1977). Algorithm as 117: The chirp discrete fourier transform of general length. *Journal of the Royal Statistical Society. Series C (Applied Statistics)*, 26(3):351–361.

Morrow, R. and Traon, P.-Y. L. (2012). Recent advances in observing mesoscale ocean dynamics with satellite altimetry. *Advances in Space Research*, 50:1062–1076.

Moskalenko, L. V. (1974). Steady state wind driven currents in the eastern half of the Mediterranean Sea. *Okianologia*, 208:491–494.

Oey, L.-Y. and Lee, H.-C. (2003). Effects of winds and caribbean eddies on the frequency of loop current eddy shedding: A numerical model study. *Journal of Geophysics Research*, 108.

Pattiaratchi, C., James, A., and Collins, M. (1986). Island wakes and headland eddies: a comparison between remotely sensed data and laboratory experiments. *Journal of Geophysics Research*, 92.

Pauluhn, A. and Chao, Y. (1999). Tracking eddies in the subtropical north-western atlantic ocean. *Physics and Chemistry of the Earth, Part A: Solid Earth and Geodesy*, 24(4):415 – 421.

Pawlak, G., MacCready, P., Edwards, K. A., and McCabe, R. (2003). Observations on the evolution of tidal vorticity at a stratified deep water headland. *Geophysical Research Letters*, 30(24).

Pérez-Santos, I., Schneider, W., Sobarzo, M., Montoya-Sánchez, R., Valle-Levinson, A., and Garcés-Vargas, J. (2010). Surface wind variability and its implications for the Yucatan basin-Caribbean Sea dynamics. *Journal of Geophysical Research: Oceans*, 115(C10).

Petersen, M. R., Williams, S. J., Maltrud, M. E., Hecht, M. W., and Hamann, B. (2013). A three dimensional eddy census of a high resolution global ocean simulation. *Journal of Geophysics Research: Oceans*, 118:1759 – 1774.

Pinardi, N. and Navarra, A. (1993). Baroclinic wind adjustment processes in the mediterranean sea. *Deep Sea Research Part II: Topical Studies in Oceanography*, 40(6):1299 – 1326.

Reguero, B. G., Losada, I. J., and Méndez, F. J. (2019). A recent increase in global wave power as a consequence of oceanic warming. *Nature Communications*, 10(1):205.

Reynolds, R. W., Rayner, N. A., Smith, T. M., Stokes, D. C., and Wang, W. (2002). An improved in situ and satellite sst analysis for climate. *Journal of Climate*, 15(13):1609–1625.

Richardson, P. L. (2005). Caribbean current and eddies as observed by surface drifters. *Deep-Sea Research II*, 52:429–463.

Rodríguez-Rubio, E., Schneider, W., and del Río, R. A. (2003). On the seasonal circulation within the panama bight derived from satellite observations of wind, altimetry and sea surface temperature. *Geophysical Research Letters*, 30(7).

Rodriguez-Vera, G., Romero-Centeno, R., Castro, C. L., and Castro, V. M. (2019). Coupled interannual variability of wind and sea surface temperature in the caribbean sea and the gulf of mexico. *Journal of Climate*, 32(14):4263–4280.

Rousset, C. and Beal, L. M. (2011). On the seasonal variability of the currents in the straits of florida and yucatan channel. *Journal of Geophysical Research*, 116.

Rudzin, J., Shay, L., Jaimes, B., and Brewster, J. K. (2017). Upper ocean observations in eastern caribbean sea reveal barrier layer within a warm core eddy. *Journal of Geophysical Research: Oceans*, 122:1057–1071.

Rudzin, J. E., Shay, L. K., and de la Cruz, B. J. (2019). The impact of the amazon–orinoco river plume on enthalpy flux and air–sea interaction within caribbean sea tropical cyclones. *Monthly Weather Review*, 147:931–950.

Sayol, J.-M., Orfila, A., Simarro, G., López, C., Renault, L., Galán, A., and Conti, D. (2013). Sea surface transport in the western mediterranean sea: A lagrangian perspective. *Journal of Geophysical Research: Oceans*, 118(12):6371–6384.

Schlax, M. G. and Chelton, D. B. (2016). The growing method of eddy identification and tracking in two and three dimensions. Technical report, College of Earth Ocean and Atmospheric Sciences, Oregon State University,.

Stammer, D. and Wunsch, C. (1999). Temporal changes in eddy energy of the oceans. *Deep-Sea Research II*, 46:77–108.

Trenberth, K. E. (1997). The definition of el niño. *Bulletin of the American Meteorological Society*, 78:2771–2777.

van der Boog, C. G., Pietrzak, J. D., Dijkstra, H. A., Brüggemann, N., van Westen, R. M., James, R. K., Bouma, T. J., Riva, R. E. M., Slobbe, D. C., Klees, R., Zijlema, M., and Katsman, C. A. (2019). The impact of upwelling on the intensification of anticyclonic ocean eddies in the caribbean sea. *Ocean Science*, 15(6):1419–1437.

Wang, G., Zhao, B., Qiao, F., and Zhao, C. (2018). Rapid intensification of super typhoon haiyan: the important role of a warm-core ocean eddy. *Ocean Dynamics*, 68:1649.

Wang, X. L. and Swail, V. R. (2001). Changes of Extreme Wave Heights in Northern Hemisphere Oceans and Related Atmospheric Circulation Regimes. *Journal of Climate*, 14:2204–2221.

Yang, F., Peng, H., Du, Y., and Wu, G. (2016). Study of the influences of warm ocean eddies on the intensity variations of tropical cyclones in the south china sea. *ISPRS International Journal of Geo-Information*, 5:169.

Zamudio, L., Leonardi, A. P., Meyers, S. D., and O'Brien, J. J. (2001). ENSO and eddies on the southwest coast of Mexico. *Geophysical Research Letters*, 28(1):13–16.